NATIONAL ADVISORY COMMITTEE FOR AERONAUTICS

REPORT 1095

TRANSONIC FLOW PAST A WEDGE PROFILE WITH DETACHED BOW WAVE

By WALTER G. VINCENTI and CLEO B. WAGONER

1952

For sale by the Superintendent of Documents, U. S. Government Printing Office, Washington 25, D. C. Yearly subscription, $9.75; foreign, $11.00; single copy price varies according to size. - - - - - - - - - Price 30 cents

REPORT 1095

TRANSONIC FLOW PAST A WEDGE PROFILE WITH DETACHED BOW WAVE

By WALTER G. VINCENTI and CLEO B. WAGONER

Ames Aeronautical Laboratory
Moffett Field, Calif.

National Advisory Committee for Aeronautics

Headquarters, 1724 F Street NW, Washington 25, D. C.

Created by act of Congress approved March 3, 1915, for the supervision and direction of the scientific study of the problems of flight (U. S. Code, title 50, sec. 151). Its membership was increased from 12 to 15 by act approved March 2, 1929, and to 17 by act approved May 25, 1948. The members are appointed by the President, and serve as such without compensation.

Conduct, under unified control, for all agencies, of scientific research on the fundamental problems of flight

REPORT 1095

TRANSONIC FLOW PAST A WEDGE PROFILE WITH DETACHED BOW WAVE[1]

By Walter G. Vincenti and Cleo B. Wagoner

SUMMARY

A theoretical study has been made of the aerodynamic characteristics at zero angle of attack of a thin, doubly symmetrical double-wedge profile in the range of supersonic flight speed in which the bow wave is detached. The analysis utilizes the equations of the transonic small-disturbance theory and involves no assumptions beyond those implicit in this theory. The mixed flow about the front half of the profile is calculated by relaxation solution of a boundary-value problem for the transonic small-disturbance equation in the hodograph plane (i.e., the Tricomi equation). The methods follow established lines except for the somewhat novel treatment of the boundary conditions along the shock polar and sonic line. The purely supersonic flow about the rear of the profile is found by means of the method of characteristics specialized to the transonic small-disturbance theory. Complete calculations were made for four values of the transonic similarity parameter. These were found sufficient to bridge the gap between the previous results of Guderley and Yoshihara at a Mach number of 1 and the results which are readily obtained when the bow wave is attached and the flow is completely supersonic.

The results of the study provide the following information as a function of the transonic similarity parameter: (1) shape and location of bow wave and sonic line, (2) chordwise distribution of Mach number and pressure, and (3) integrated pressure drag of front wedge, rear wedge, and complete profile. The results show that the local Mach number at a fixed point on a profile of given thickness ratio increases monotonically as the free-stream Mach number increases from 1. In agreement with other recent findings, this increase is at first very slight for a considerable increment away from the sonic flight condition. The coefficient of pressure drag for the complete profile varies relatively slightly near the sonic flight speed, decreases rapidly in the vicinity of bow-wave attachment, and then decreases at a progressively less rapid rate in the range of purely supersonic flow.

INTRODUCTION

At supersonic flight speeds, the flow field about a wedge of nfinite span is characterized at zero angle of attack by a symmetrical, two-dimensional shock wave. This wave, which forms either on or in front of the apex of the wedge, is called the bow wave in recognition of its analogy to the surface wave which forms at the bow of a moving ship. As is well known, the shape of the bow wave and the nature of the flow about the wedge vary depending upon the apex angle of the wedge and the Mach number of the free stream. Consider, for simplicity, the case of a wedge of fixed angle. It will be assumed that the wedge is perfectly sharp and that the effects of viscosity are negligible. It will also be assumed that the wedge is of finite length in the streamwise direction. Under these circumstances, three essentially different regimes of flow are possible, depending on the Mach number of the free stream:

1. Attached bow wave with purely supersonic flow: Above a certain free-stream Mach number, the value of which depends on the magnitude of the wedge angle, the bow wave is attached to the apex of the wedge, and the local flow at all points downstream of the wave is supersonic. Under these conditions, the velocity at the surface of the wedge is uniform, and the bow wave is straight out to its point of intersection with the first Mach wave from the downstream end of the wedge. This regime of purely supersonic flow was first studied by Prandtl and Meyer as long ago as 1908 (reference 1) and is now to be found analyzed in any standard text on gas dynamics.

2. Attached bow wave with mixed subsonic and supersonic flow: As the free-stream Mach number is reduced in the purely supersonic regime, a condition is eventually reached at which the local velocity downstream of the straight portion of the bow wave is exactly sonic. With further reduction in Mach number, the flow in the vicinity of the wedge becomes subsonic, and the entire fundamental nature of the flow field is altered. For a small range of free-stream Mach number, the bow wave remains attached to the apex, but the velocity along the surface of the wedge is now nonuniform. The wave itself, though still inclined toward the rear at all points, is now curved starting from its beginning at the apex. The rather complex sequence of events in this particular regime of mixed subsonic and supersonic flow has been clarified by Guderley (reference 2), but no specific calculations have been made. Since the regime prevails over only a narrow range of Mach number, the lack of quantitative information is not of serious consequence.

3. Detached bow wave: At a free-stream Mach number slightly below that which gives sonic flow behind the bow

[1] Supersedes NACA TN 2339, "Transonic Flow Past a Wedge Profile With Detached Bow Wave—General Analytical Method and Final Calculated Results" by Walter G. Vincenti and Cleo B. Wagoner, 1951, and NACA TN 2588, "Transonic Flow Past a Wedge Profile With Detached Bow Wave—Details of Analysis" by Walter G. Vincenti and Cleo B. Wagoner, 1951.

234239—53

wave, a limiting condition is reached below which an attached wave is no longer possible. At lower Mach numbers, therefore, the wave detaches from the apex and stands in the stream forward of the wedge. In this regime of flow, which prevails down to a Mach number of 1, the subsonic flow over the surface of the wedge has a stagnation point at the apex. The element of the curved bow wave directly ahead of the apex is now normal to the direction of the free stream. This regime of mixed flow may occupy a considerable interval of Mach number in the currently important range of transonic flight speeds. Because of difficulties inherent in the mathematics of the problem, however, quantitative theoretical results free of special assumptions are generally lacking.

Perhaps the first calculations of the flow about a finite wedge with detached bow wave were made by Maccoll and Codd in England between 1938 and 1942 (reference 3) and were reported by Maccoll at the 6th International Congress of Applied Mechanics in Paris in 1946 (reference 4). In this initial work, the computations were carried out in the plane of physical coordinates—or, more precisely, in a plane of distorted physical coordinates. For reasons which will appear later, a direct solution was not possible with this approach, so that recourse was had to a method of successive approximations. The successive approximations were obtained by numerical integration of the partial differential equations of fluid motion in the subsonic portion of the flow field. By this means Maccoll and Codd were able to obtain results for the mixed flow about bodies of various shape. The calculations for the wedge with a detached wave were confined, however, to the single case of a free-stream Mach number of 1.5 and a total wedge angle of 40°.

An alternative method of analysis, which eliminates the need for successive approximations, has been described independently by Frankl (1945) in Russia and by Guderley (1947) in this country (references 5 and 2, respectively). In this approach, the problem of the wedge with detached wave is formulated as a boundary-value problem with the velocity components as the independent variables. Using this hodograph method, Frankl was able to prove that the solution of the detached-wave problem is unique. (This had been tacitly assumed by Maccoll and Codd.) Guderley, following a similar approach, showed how the hodograph problem can be simplified by restriction to small disturbances about the sonic velocity. These developments have been subsequently reviewed in nonmathematical form by Busemann (reference 6). More recently (1949), Guderley and Yoshihara, using the small-disturbance theory, have obtained a quantitative solution for the finite wedge at a free-stream Mach number of 1 (reference 7). In this special limiting case, the bow wave disappears at infinity upstream, which facilitates the mathematical analysis. The corresponding boundary-value problem in the hodograph plane was solved analytically by Guderley and Yoshihara with the aid of Fourier analysis and a harmonic analyzer. For free-stream Mach numbers greater than 1, a comparable analytical solution of the boundary-value problem is not yet available. Such a solution would appear, indeed, to present serious mathematical difficulties, even in the relatively simple small-disturbance theory.

The work described in the present report is a logical extension and application of the hodograph method of Guderley and Frankl. To circumvent the lack of an analytical solution at Mach numbers greater than 1, it was proposed in the present study to solve the boundary-value problem by means of numerical techniques. In the application of numerical methods, the present work has much in common with the investigations of Maccoll and Codd. The use of the hodograph approach, however, eliminates the need for successive approximations and brings about other improvements in ease and rigor. Furthermore, through use of the similarity principles inherent in the small-disturbance theory, general results applicable to any thin wedge can be obtained on the basis of a relatively small number of specific calculations. In the present work, these results are used, in particular, to study the pressure distribution and drag of a complete, doubly symmetrical double-wedge profile in the range of flight Mach numbers from unity upwards. The report is divided into two major parts. Part I contains a nonmathematical description of the theoretical problem and a detailed discussion of the final results. This portion of the report can be read without reference to part II, which explains the details of the mathematical procedures.

Since the completion of the present calculations, experimental studies of the wedge problem have been reported by Bryson in reference 8 and by Griffith in reference 9. Certain of the results which appear in Bryson's report were also given in preliminary form by Liepmann and Bryson in reference 10.

NOTATION

PRIMARY SYMBOLS

a_*	critical velocity (i. e., velocity at which the velocity of flow and the velocity of sound are equal)
c	airfoil chord
c_d	drag coefficient $\left(\frac{\text{drag per unit span}}{q_o c}\right)$
$\tilde{c}_d$	generalized drag coefficient $\left\{\left[\frac{(\gamma+1)^{1/3}}{(t/c)^{5/3}}\right] c_d\right\}$
C_p	pressure coefficient $\left(\frac{p-p_o}{q_o}\right)$
$\tilde{C}_p$	generalized pressure coefficient $\left\{\left[\frac{(\gamma+1)^{1/3}}{(t/c)^{2/3}}\right] C_p\right\}$
e,f,h,k	length of irregular lattice intervals relative to that of basic interval
$f\left(\frac{x}{c}\right)$	function defining shape of profile
$F(\lambda)$, $G(\lambda)$	functions defined along sonic line in hodograph (See equation (23).)
I_m	integral defined by equation (56)
J_i	($i=1,2,3$) component integrals (See equation (50) et seq.)
K,L	functions of e, f, and $\bar{\eta}_o$ (See equation (44).)
k_1,k_2	numerical constants (See equations (24) and (32).)
M	Mach number
p	static pressure
q	dynamic pressure $\left(\frac{\gamma}{2} pM^2\right)$

$S(\tilde{\eta})$	function defined by equation (41)
t	airfoil thickness
V	local speed of flow
x,y	Cartesian coordinates
Y	ordinate function $\left\{\left[(\gamma+1)\left(\frac{t}{c}\right)\right]^{1/3}\left(\frac{y}{c}\right)\right\}$
β	absolute value of $\tilde{\eta}$ at left-hand limit of lattice
γ	ratio of specific heats (1.4 for air)
Δ	basic lattice interval
η	hodograph variable defined by equation (18)
θ	local inclination of flow relative to x axis
θ'	variable of integration (See equation (25).)
θ_w	half-angle of wedge
$\tilde{\Theta}_u,\tilde{\Theta}_d$	ordinates of upgoing and downgoing characteristics at $\tilde{\eta}=0$
λ	hodograph variable (See equation (23).)
ξ	speed function $\left\{\frac{M^2-1}{[(\gamma+1)(t/c)]^{2/3}}\right\}$
ξ_o	transonic similarity parameter $\left\{\frac{M_o^2-1}{[(\gamma+1)(t/c)]^{2/3}}\right\}$
ρ	fluid density
ψ	stream function
ψ_E	value of ψ at the point E (See equation (33).)

SUBSCRIPTS

o	conditions in free stream
0,1,2, etc.	value at a prescribed lattice point
*	conditions at critical speed
f	front portion of airfoil
r	rear portion of airfoil
$M_o=1$	value at free-stream Mach number of 1
$\xi_o=0$	value at $\xi_o=0$

SUPERSCRIPT

$(\tilde{\ })$	quantity in normalized form (See equation (26).)

PART I—GENERAL METHOD AND FINAL RESULTS

GENERAL ANALYTICAL METHOD

DESCRIPTION OF FLOW FIELD

It is convenient to begin by examining the nature of the flow field which exists around a doubly symmetrical, double-wedge profile when the bow wave is detached. The complete double-wedge profile is considered here since the determination of the characteristics of this profile is the final object of the present work. The description and results relative to the flow over the forward half of this profile, however, are applicable, within minor limitations, to the flow over any finite wedge which terminates in a sharp convex corner. It will be assumed in all that follows that the fluid surrounding the profile is a perfect gas and that the effects of viscosity and thermal conductivity are negligible.

Under these idealized conditions, the flow about a nonlifting double-wedge profile with a detached bow wave is qualitatively as shown in figure 1. (Since the flow is symmetrical about the chord line, only the upper half of the field is shown.) As indicated, the subsonic flow which exists

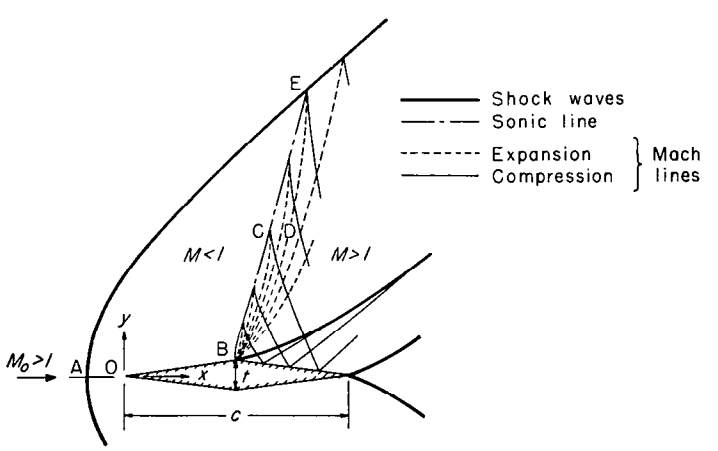

FIGURE 1.—Flow about double-wedge profile with detached bow wave.

behind the detached wave is confined to a limited region bounded by the wave, the sonic line, and the forward half of the profile. The fluid which enters this region is decelerated discontinuously from supersonic to subsonic velocity in passing through the detached shock wave. Downstream of the shock wave, the fluid is accelerated continuously, first to the speed of sound at the sonic line and then to supersonic speed beyond this line. As previously mentioned, the detached wave begins normal to the free stream at the axis of symmetry (point A) and curves progressively downstream. Far from the airfoil, the slope of the wave tends asymptotically to the slope of a free-stream Mach line. Since the detached wave is curved, the flow behind the wave is, of course, nonuniform. The sonic line, which forms the downstream boundary of the subsonic region, begins at the ridge of the profile (point B) and extends to some point E on the shock wave. Since the flow in the subsonic region is nonuniform, the sonic line is curved. As can be demonstrated, however, it must leave the ridge normal to the forward surface of the profile.

Directly to the rear of the sonic line at the ridge, a supersonic expansion fan originates. This expansion fan tends, in the immediate vicinity of the ridge, toward a simple Prandtl-Meyer flow, in which the sonic line and the elementary Mach waves would be straight lines emanating radially from the corner. Since the sonic line in the present flow is curved, however, the Mach waves of the expansion fan must be curved as well, the curvature being in the forward direction. By virtue of this forward curvature, certain of the expansion waves meet the sonic line, while others meet the outer portion of the bow wave. One particular expansion wave BDE meets both the sonic line and the bow wave at their common point E. This particular wave may be termed the "separating wave," since it separates the expansion waves into two classes: those which reach the sonic line and those which do not. It is apparent that any small disturbance introduced into the expansion fan forward of the separating wave BDE will travel along a Mach wave to a point on the sonic line. From there it will spread throughout the subsonic region, thereby influencing the shape of the sonic line, and, hence,

of the expansion fan itself. The entire subsonic region and the limited portion BDECB of the adjacent supersonic region are thus interdependent and must be regarded for analytical purposes as a single, bounded transonic zone. A small disturbance originating in the purely supersonic region to the rear of the separating wave BDE cannot reach the sonic line and can have no effect upon the flow in the aforementioned transonic zone.

The supersonic flow over the rear of the airfoil is directly influenced by conditions in the transonic part of the field. Analysis indicates that the elementary expansion waves which reach the sonic line do not terminate there but are reflected as elementary compression waves. These waves are again reflected as compression waves at the solid surface of the airfoil. After this last reflection, the elementary compression waves coalesce to form an oblique shock wave which begins at the ridge. On thin sections this shock wave is very weak and may be regarded, for all practical purposes, as a distributed compression. Rearward of the oblique wave from the ridge, the flow continues with supersonic velocity to the trailing edge, where there is a second oblique shock wave of the type familiar from purely supersonic airfoil problems.

METHOD OF ANALYSIS

To handle the present problem analytically, the flow must first be determined in the transonic zone bounded by the bow wave, the airfoil profile, and the separating Mach wave. As in all transonic problems, such determination involves the solution of a partial differential equation of mixed type, that is, one which is elliptic in the subsonic region and hyperbolic in the adjoining supersonic region. The solution of an equation of this type is troublesome at best. In the present problem, however, additional difficulties arise. First of all, the differential equation, beside being of the mixed type, is also nonlinear. Second, the location of two of the boundaries of the transonic zone—the bow wave and the separating Mach wave—is not known a priori but must be determined as part of the solution. Third, the flow in the transonic zone, having passed through the curved bow wave, is necessarily rotational.

The foregoing difficulties seriously complicate any attempt to solve the problem in the physical plane, even when numerical techniques are employed. The nonlinearity of the differential equation, though it does not preclude a solution by numerical methods, does greatly increase the amount of numerical work over that which is ordinarily encountered with a linear equation. The lack of knowledge concerning the location of the boundaries of the transonic zone can be overcome by resorting to a method of successive approximations, as in the work of Maccoll and Codd (references 3 and 4). Such a procedure, however, entails considerably more labor than would be required if the boundaries were known at the outset.[2] The difficulties due to the fluid rotation can be disposed of by simply assuming that the rotation is negligible. The inaccuracies introduced by this assumption are undoubtedly small, except for thick wedges moving at relatively high Mach numbers. Even with the rotation eliminated from the equations, however, the basic nonlinearity still remains.

In addition to the theoretical difficulties just discussed, there exists a practical complication which is important from the computational point of view. This complication arises from the fact that any rigorous solution of the problem must be a function of three independent variables: the free-stream Mach number M_o, the thickness ratio t/c, and the ratio of specific heats γ. Thus, if a rigorous theory is used, a considerable number of cases must be calculated to obtain an adequate cross section of numerical results.

As in the work of Guderley and Frankl (references 2 and 5), the first step in the solution of the problem is to transform the flow from the physical plane to the hodograph plane. This affords an immediate simplification by providing a completely fixed set of boundaries for the transonic zone. The bow wave, in particular, goes over into a known shock polar, while the separating Mach wave transforms into one of the fixed epicycloids which make up the characteristic net in the hodograph. The differential equation in the hodograph variables is still of the mixed type, as would be expected in view of the transonic nature of the original problem. The equation is also still nonlinear if the fluid rotation is included in the analysis. If the rotation is arbitrarily neglected, however, the differential equation in the hodograph becomes linear, in contrast to the previous situation in the physical coordinates.[3] Since the fundamentals of the problem are unchanged by the transformation to the hodograph, the complication still remains that any solution must be a function of the three variables mentioned above.

The second major step in the analysis is to introduce the assumption of small disturbances. Specifically, it is assumed that the entire flow field, including the free stream, differs only slightly from a parallel flow at the critical speed a_*.[4] As is well known, this small-disturbance approximation brings about important simplifications in the mathematics of the problem. First, the terms representing fluid rotation turn out to be of the same order as other terms which are neglected in the analysis. This means that the use of the linear differential equation in the hodograph is strictly justified within the framework of the approximate theory. Second, the differential equation itself, though still of mixed type, takes on an especially simple form (the Tricomi equation). This equation has been the subject of consid-

[2] Maccoll and Codd simplify both the fundamental problem and the calculative procedure by taking the sonic line, instead of the separating Mach wave, as the downstream limit of the region of calculation. This eliminates the need for considering the mathematical singularity which exists behind the sonic line at the ridge, but requires in return that some condition be specified along the sonic line itself. This requirement is met by assuming that the streamlines and the sonic line are mutually perpendicular and that the sonic line may be represented by a suitable parabola. The error introduced by these special assumptions is not known, but would probably be considerable for thin wedges at low supersonic speeds.

[3] Frankl's uniqueness proof, mentioned in the introduction, is based on the linear equation and thus ignores the fluid rotation. It seems unlikely, however, that the inclusion of rotational effects would alter the conclusions of the study.

[4] As discussed in several recent papers (see, for example, references 11 and 12), the theory can also be formulated in terms of differences relative to the free-stream speed V_o. This latter, less restrictive formulation reveals clearly the relationship which exists between the transonic small-disturbance theory and the familiar linear theory of subsonic or supersonic flow. As shown by Spreiter (see page 9 of reference 12), an a_* analysis will yield results identical to those of a V_o analysis provided the similarity parameter and pressure coefficient in the former case are taken as in equations (1) and (7) below. If this procedure is followed, the results of the a_* analysis may even be expected to tend toward those of linear theory as the free-stream Mach number increases or decreases from 1. (An analytical example of just this behavior has been given by Bryson in appendix A of reference 8.) It appears, therefore, that the a_* formulation, when suitably used, gives results of wider theoretical validity than would be anticipated on the basis of its own rather restrictive underlying assumption.

erable mathematical study, beginning with the work of Tricomi (reference 13). Third, the solution of the problem becomes a function of a single parameter which involves all three of the individual variables previously discussed. This is the so-called transonic similarity parameter ξ_o which can be written

$$\xi_o=\frac{M_o^2-1}{[(\gamma+1)(t/c)]^{2/3}} \tag{1}$$

This last simplification greatly reduces the amount of computation required to investigate the effects of changes in the individual variables.

It may be remarked in passing that the assumption of small disturbances will obviously be violated near the stagnation point which exists at the leading edge of the profile. A similar situation is, of course, encountered in the classical theory of thin airfoils at purely subsonic speeds. There the inconsistency is known to be of little practical consequence except in the immediate vicinity of the leading edge itself. It is to be expected that the same result will prevail in the locally subsonic flow encountered here.

A detailed account of the formulation and solution of the boundary-value problem in the hodograph plane is given in part II of the present report. Suffice it here to say that the boundaries and boundary conditions are taken essentially as given by Guderley (reference 2), except that the supersonic portion of the transonic zone is replaced by an equivalent integral relation which must be satisfied everywhere along the sonic line. By this modification, which involves no approximations beyond those already employed, the mathematical problem is reduced to that of solving a purely elliptic differential equation. This was found essential to the numerical solution of the problem. The numerical solution itself is carried out in more or less standard fashion by means of finite-difference equations and relaxation techniques.[5]

Once the solution for the front half of the airfoil is determined in the hodograph plane, the transformation back to the physical plane is a simple matter. The purely supersonic flow over the rear half is then constructed in the physical plane by means of the method of characteristics as specialized to the small-disturbance theory.

It will be noted that the solution of the problem in the present manner, though laborious because of the use of numerical techniques, requires no special assumptions beyond those implicit in the differential equations. In particular, no restrictions are necessary with regard to the geometric shape of the shock wave or sonic line.

Although the transonic small-disturbance theory was originally formulated for the solution of problems of mixed flow, it is not confined in its applications to problems in which such flow actually occurs. The theory may still be applied—in simple analytical form, in fact—in the completely supersonic regime, where the bow wave is attached and the region of subsonic flow has disappeared. This is accomplished by first reducing the complete equations for the oblique shock wave and the Prandtl-Meyer expansion to appropriate forms involving the transonic similarity parameter (see, for example, the work of Tsien and Baron, reference 14) and then applying these results as in the standard shock-expansion method. This procedure is applicable to the present airfoil when $\xi_o\geqq 2^{1/3}=1.260$, this being the condition, to the order of accuracy of the small-disturbance theory, for an attached wave with not less than sonic flow on the downstream side.[6] (Consistent with the remarks in the introduction, attachment of the wave itself takes place at the somewhat lower value of $\xi_o=3/(4)^{2/3}=1.191$.)

RESULTS AND DISCUSSION

Calculations have been carried out, according to the methods described in the preceding section, for four values of the similarity parameter ξ_o; namely, 0.484, 0.703, 0.921, and 1.058. These four cases were found sufficient to bridge the gap between the findings of Guderley and Yoshihara at $M_o=1$ ($\xi_o=0$) and the analytical results which are available when the bow wave is attached and the flow is everywhere supersonic ($\xi_o\geqq 1.260$). The complete results are given in figures 2 through 8 and are described in the following paragraphs.

BOW WAVE AND SONIC LINE

The dimensionless ordinates y/c of any chosen line which intersects the streamlines are given in the transonic small-disturbance theory by an equation of the form

$$[(\gamma+1)(t/c)]^{1/3}\left(\frac{y}{c}\right)=Y\left(\frac{x}{c},\,\xi_o\right) \tag{2}$$

where Y is a function of the dimensionless abscissa x/c and the similarity parameter ξ_o. (For derivation of the transonic similarity rules on which these and later equations are based, see references 11, 12, 15, 16, or 17.) The calculated shape of the bow wave and sonic line is shown in figure 2 in the form prescribed by the foregoing equation.

To facilitate the discussion, it will sometimes be convenient to look upon a generalized plot, such as that of figure 2, as applying to fixed values of t/c and γ. From this point of view, a decrease toward zero in the similarity parameter can be thought of as simply a decrease toward 1 in the free-stream Mach number. In figure 2 an appreciation of physical proportions is further achieved by dividing Y by the numerical factor $(0.24)^{1/3}$ and plotting the results to equal vertical and horizontal scales. Thus, for the specific conditions of $t/c=0.10$ and $\gamma=1.4$ (air), the vertical scale reads directly in values of y/c, and the figure provides as it stands a geometrically correct representation of the flow field. The corresponding values of M_o are given by the upper figure along the shock wave. (The sonic velocity will first appear in the flow field about the 10-percent-thick section at a free-stream Mach number of approximately 1.219 ($\xi_o=1.260$). Detachment of the shock wave will occur at the slightly lower Mach number of 1.208 ($\xi_o=1.191$).)

[5] As is often the case with relaxation work, the numerical calculations made considerable demands upon the skill and perseverance of the computer. Special credit is due Mrs. Helen Mendel for the successful completion of this phase of the study.

[6] In the shock-expansion method it is assumed that the pressure is uniform on each straight-line segment of the airfoil surface. Because of interaction effects between the shock wave from the bow and the expansion fan from the ridge, this condition is not completely fulfilled until the flow behind the bow wave is somewhat greater than sonic, that is, until the value of ξ_o is somewhat above 1.260. In conformity with usual practice, this complication is ignored in the present work since it is known to have only a negligible influence upon the computed characteristics of the airfoil.

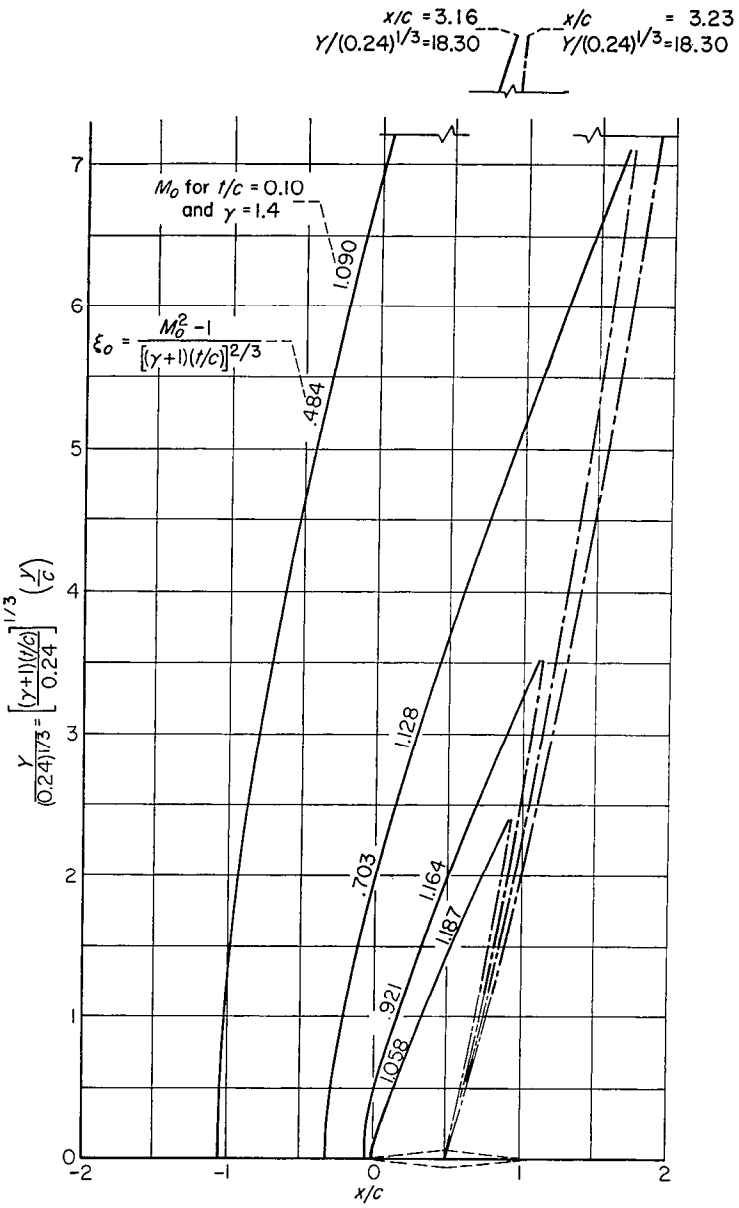

FIGURE 2.—Shape of bow wave and sonic line.

The dashed outline of the airfoil which appears in figure 2 is to be regarded as a diagrammatic representation only. In a similarity plot of this kind, the profile must be regarded, properly speaking, as coinciding with the horizontal axis. (For a more complete discussion of this point see page 29 of reference 18.) The dashed profile in figure 2 is included only as an aid in orienting the reader.

It will be noted that in each case in figure 2 the shock wave and sonic line as calculated do not meet at a common point. This discrepancy appears in the course of the transformation from the hodograph to the physical plane; it is primarily a reflection of the fact that a solution of the system of finite-difference equations in the hodograph is not an exact solution of the boundary-value problem for the original partial differential equation. This so-called "truncation error" can, in principle, be made as small as desired by progressively decreasing the mesh size in the hodograph. In the present work this procedure has been carried in each case to the point where increased refinement caused only an insignificant change in the pressure distribution or over-all drag. Because of the nature of the hodograph transformation, however, the details of the accompanying flow field are subject to somewhat greater error, particularly with regard to the over-all height of the subsonic region. As implied by the size of the gap between the shock wave and sonic line, the absolute magnitude of this error increases as ξ_o decreases, though the percentage error in terms of the height of the subsonic region is nearly constant. The actual magnitude of the truncation error is in all cases certainly less than the errors caused by the basic theoretical assumption of small disturbances.

It is seen in figure 2 that in each case the calculated sonic line begins at the midchord point at right angles to the horizontal axis. This result is consistent, to the accuracy of the small-disturbance theory, with the known fact that the sonic line given by any rigorous treatment would leave the ridge normal to the forward surface of the profile. As it leaves the airfoil, the sonic line curves at first rather sharply toward the rear. The initial curvature can, in fact, be shown to be infinite. A short distance from the airfoil the rearward trend is reversed, with the result that the sonic line has a predominately forward curvature over most of its length. The flow across most of the sonic line in the present problem is apparently analogous to the accelerating transonic flow through a continuous-walled, converging-diverging nozzle, where the sonic line is known to have a consistently forward curvature. The rearward curvature which is evident close to the airfoil is only a localized effect caused by the presence of the sharp corner at the ridge.

The rapidity with which the subsonic region expands vertically with reduction in the free-stream Mach number is striking. For the airfoil of 10-percent thickness ratio, for example, the semiheight of the subsonic region in figure 1 grows from approximately 2.4 chord lengths at $M_o=1.187$ to approximately 18.3 chord lengths at $M_o=1.090$. The height of the subsonic region (and the distance of the shock wave ahead of the airfoil) would, of course, tend to infinity as the Mach number approached still closer to unity. These results imply that the tip effects are likely to be considerable on finite-span wings at free-stream Mach numbers close to 1.

According to the transonic similarity rules, the speed of flow at any point in the generalized flow field is determined by the local value of a dimensionless speed function ξ, which can be written

$$\xi=\frac{M^2-1}{[(\gamma+1)(t/c)]^{2/3}} \tag{3}$$

where M is the local value of the Mach number. (The transonic similarity parameter is thus merely the special value of the speed function which applies at points in the free stream.) As a matter of interest, contours of constant speed function ξ in the region between the shock wave and sonic line have been determined for the case of $\xi_o=0.921$. These results are shown in figure 3. By virtue of equation (3), the contours of constant ξ may be interpreted, for fixed values of t/c and γ, as contours of constant Mach number. They may also be regarded, to the order of accuracy of the transonic small-disturbance theory, as contours of constant velocity, pressure, density, and temperature. It will be

noted that certain of the contours, in common with the sonic line, fail to meet the shock wave. This is again a reflection of errors inherent in the finite-difference solution.

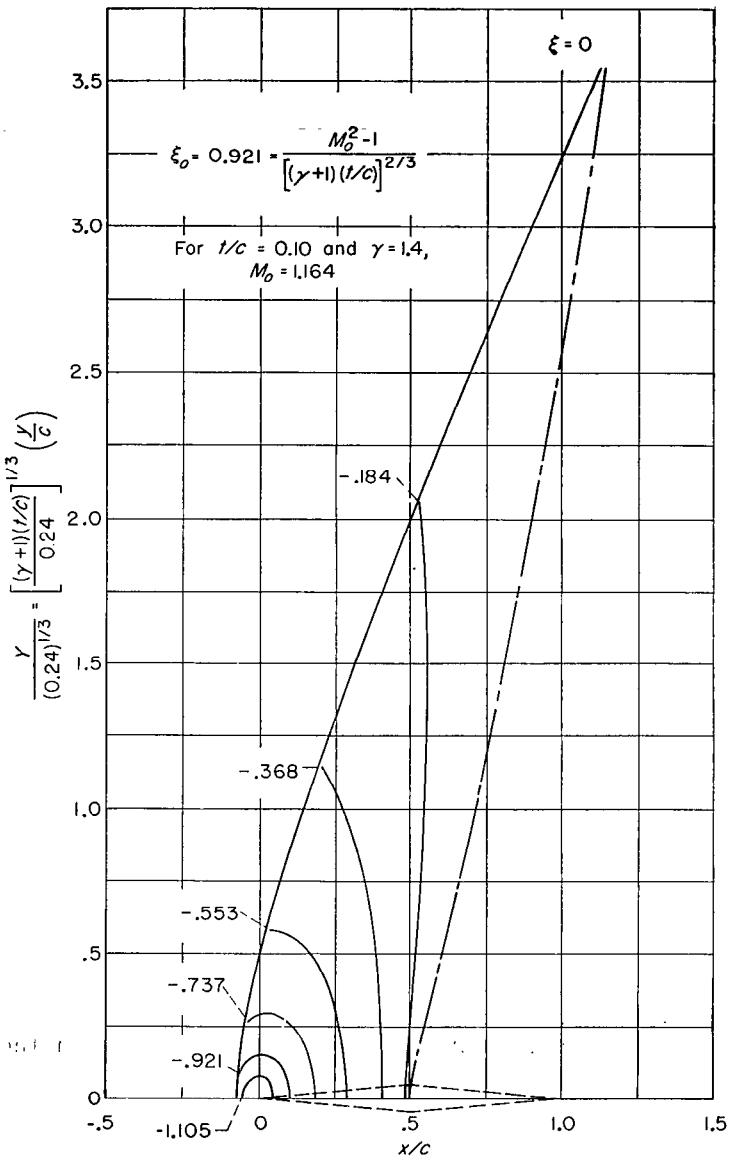

FIGURE 3.—Contours of constant speed function for ξ_o=0.921.

CHORDWISE DISTRIBUTION OF MACH NUMBER AND PRESSURE

At points on the surface of the airfoil, the speed function ξ is related to the similarity parameter ξ_o by an equation of the form

$$\xi = \xi\left(\frac{x}{c}, \xi_o\right) \tag{4}$$

The calculated values of ξ at the surface of the airfoil are shown in figure 4 for the four values of the similarity parameter. Also included in the figure are results for ξ_o=0 as obtained from the previously cited work of Guderley and Yoshihara (reference 7). In line with the earlier interpretation, the curves of figure 4 may be looked upon here as representing the chordwise distribution of Mach number for fixed values of t/c and γ but different values of M_o.

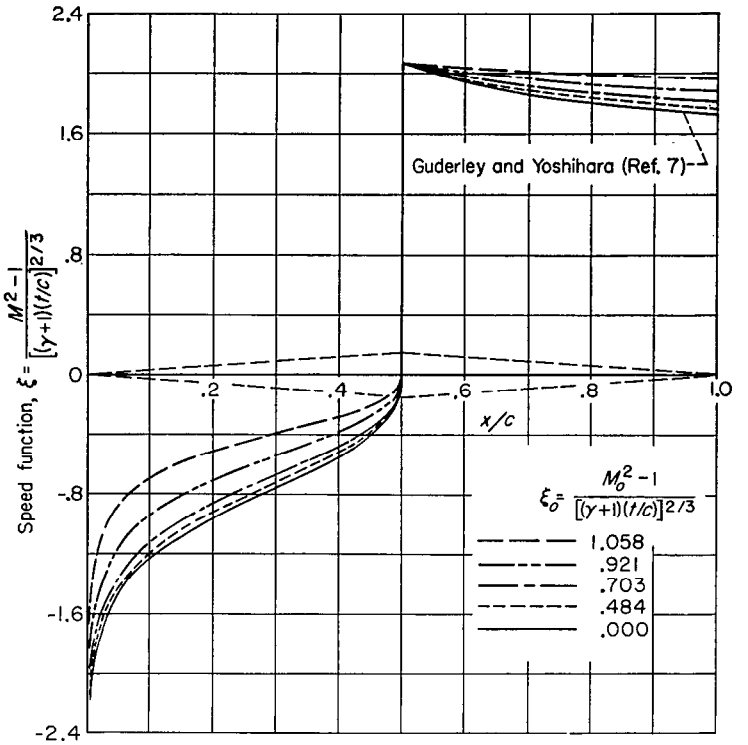

FIGURE 4.—Chordwise distribution of speed function at surface of airfoil.

All of the distribution curves of figure 4 have the same general shape. In each case, for example, the calculated Mach number at the leading edge has an infinite negative value. This physically impossible result, which is characteristic of small-disturbance theories in general, represents the stagnation condition which must prevail in the real subsonic flow at the leading edge. Rearward from the leading edge, the Mach number in each case rises more or less rapidly to the prescribed value of unity on the forward side of the ridge. Turning the corner at the ridge, the flow expands discontinuously to a supersonic Mach number which, for given values of t/c and γ, is independent of conditions in the free stream. Over the rear half of the airfoil, the Mach number decreases slightly as a result of the compression waves reflected from the sonic line (see fig. 1). In general, for an airfoil of fixed thickness ratio, increasing the free-stream Mach number from unity brings about an increase in the average local Mach number over both the front and rear surfaces of the profile.

The nature of this latter variation is illustrated more clearly in figure 5, which is a cross plot of ξ versus ξ_o for the 25- and 75-percent chordwise stations. The short vertical lines labeled S at ξ_o=1.260 denote the point at which the transonic small-disturbance theory predicts an attached bow wave with uniform sonic flow over the forward half of the profile. Results at this point and at all points to the right of S can be determined analytically as explained earlier in the text. It is apparent from figure 5 that the values given by the present numerical work satisfactorily bridge the gap which would otherwise exist between the analytical results at either side.

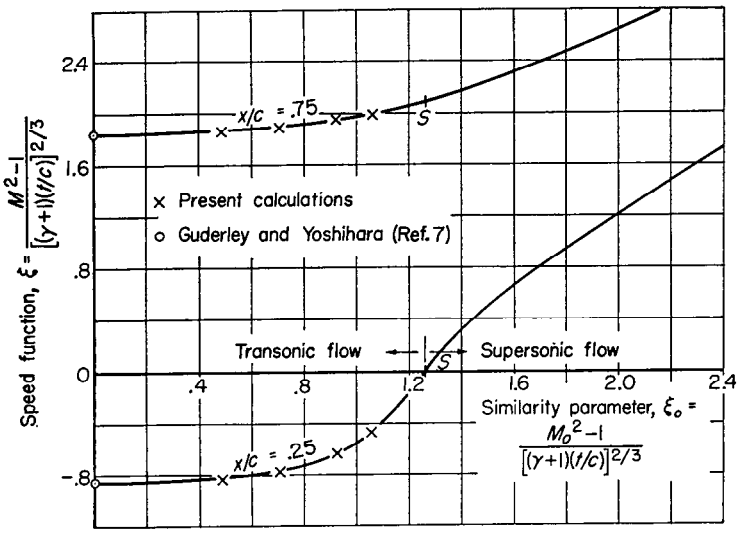

FIGURE 5.—Variation of speed function at 25- and 75-percent chordwise stations.

As can be seen from figure 5, the change in local conditions with change in free-stream Mach number is slight for a considerable distance away from a free-stream Mach number of 1. The curves of this figure have, in fact, been drawn with a horizontal tangent at $\xi_o=0$. This is in accord with Guderley's recent analytical study of two-dimensional flows with a free-stream Mach number close to 1 (reference 19). Guderley's results indicate that just at the sonic flight speed the local Mach number at any point on an arbitrary two-dimensional profile is stationary with respect to variations in the free-stream Mach number, that is,

$$\left(\frac{dM}{dM_o}\right)_{M_o=1}=0 \tag{5}$$

In terms of the present variables (see equations (1) and (3)) this requires that

$$\left(\frac{d\xi}{d\xi_o}\right)_{\xi_o=0}=0 \tag{6}$$

The same results were anticipated by Liepmann and Bryson on the basis of the physical considerations presented in reference 10.

The pressure coefficient $C_p \equiv (p-p_o)/q_o$ is given in the transonic small-disturbance theory by the equation

$$\frac{(\gamma+1)^{1/3}}{(t/c)^{2/3}} C_p=-2(\xi-\xi_o) \tag{7}$$

At points on the surface of the airfoil, equation (4) applies for ξ, so that equation (7) there has the form

$$\frac{(\gamma+1)^{1/3}}{(t/c)^{2/3}} C_p=\tilde{C}_p\left(\frac{x}{c}, \xi_o\right) \tag{8}$$

where $\tilde{C}_p$ is a generalized pressure coefficient which depends only on x/c and ξ_o. The values of $\tilde{C}_p$ for the double-wedge section, as calculated by means of equation (7), are shown in figure 6. The curves here are essentially the same as the curves of ξ in figure 4, except that they are inverted and shifted vertically by an amount which differs for each curve. It can be seen from this figure that as the free-stream Mach number increases above 1 the pressure distribution tends toward the well-known supersonic type of distribution in which the pressure is uniform over each surface of the profile.

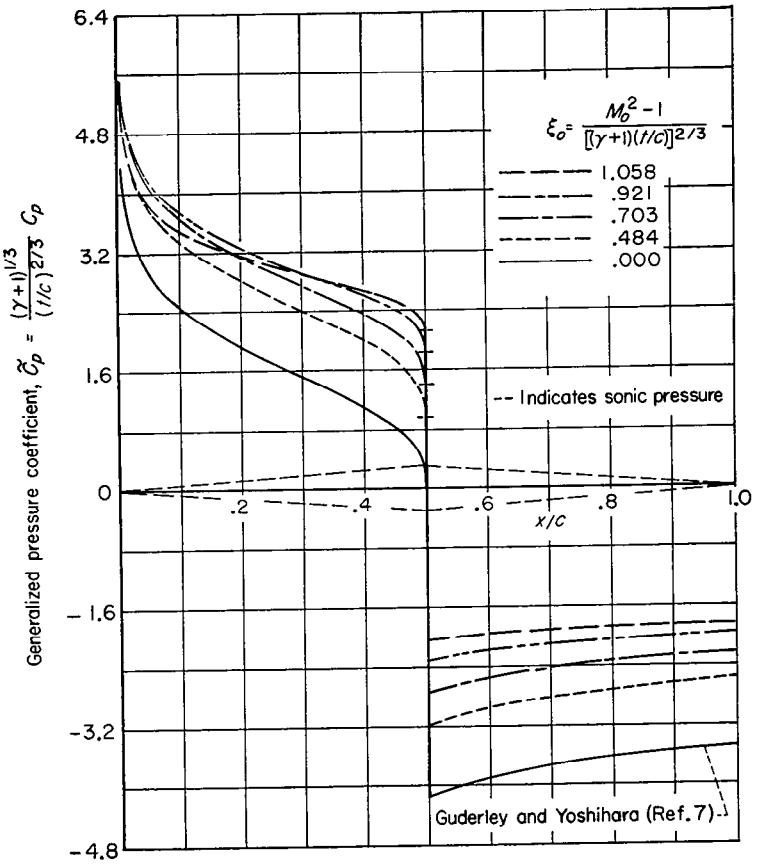

FIGURE 6.—Chordwise distribution of generalized pressure coefficient at surface of airfoil.

PRESSURE DRAG

Let the ordinates of a general profile be represented by the equation $y/c=(t/c)\,f(x/c)$. With the aid of equation (8), the pressure-drag coefficient can then be written in the generalized form

$$\frac{(\gamma+1)^{1/3}}{(t/c)^{5/3}} c_d=\oint \tilde{C}_p\left(\frac{x}{c}, \xi_o\right) f'\left(\frac{x}{c}\right) d\left(\frac{x}{c}\right)=\tilde{c}_d(\xi_o) \tag{9}$$

where $f'(x/c)$ is the derivative of $f(x/c)$ with respect to its argument and the integration is performed around the profile in the clockwise direction. In the specific case of the double-wedge profile, the ordinates of the front wedge are given by $y/c=\pm(t/c)(x/c)$. The portion of the generalized drag coefficient contributed by this half of the profile is thus

$$\tilde{c}_{d_f}=\frac{(\gamma+1)^{1/3}}{(t/c)^{5/3}} c_{d_f}=2\int_0^{1/2} \tilde{C}_p\, d\left(\frac{x}{c}\right) \tag{10a}$$

where, because of symmetry, the integration need be performed over only the upper surface. For the rear wedge the ordinates are given by $y/c=\pm(t/c)(1-x/c)$, and the corresponding portion of the generalized drag coefficient is

$$\tilde{c}_{d_r}=\frac{(\gamma+1)^{1/3}}{(t/c)^{5/3}} c_{d_r}=-2\int_1^{1} \tilde{C}_p\, d\left(\frac{x}{c}\right) \tag{10b}$$

In the present study the integrals in equations (10) were evaluated by mechanical integration of the pressure-distribution curves of figure 6. In the case of $\bar{c}_{d_f}$, a small, analytically determined allowance was included for the effect of the singularity at the leading edge. The final results are shown in figure 7. The drag coefficient of the complete airfoil was obtained, of course, by adding the drag coefficients for the front and rear wedges.

The results of figure 7 indicate that at a flight Mach number of 1 approximately two-thirds of the drag of the section is contributed by the rear wedge. As the Mach number increases from 1, the drag coefficient of this portion of the profile decreases continuously. At the same time, the drag coefficient of the front wedge first increases until it is considerably above that of the rear half, after which it also decreases. At a sufficiently high free-stream Mach number, the drag coefficient of each half of the airfoil is essentially the same. As a result of the difference in the drag variation of the two halves, the drag coefficient of the complete profile shows little variation for some distance above a Mach number of 1. As the shock wave attaches to the leading edge, however, and the local flow becomes everywhere supersonic, the total drag coefficient drops markedly. Far into the supersonic regime the variation is again less rapid.

The curve for the front wedge in figure 7 has been continued into the subsonic range of flight speeds ($\xi_0<0$) by the analytical work of Cole (reference 20). The continued curve decreases monotonically toward zero as the value of ξ_0 is reduced. The continuation of the curve for the rear wedge has been accomplished by Trilling (reference 21). This curve apparently reaches a maximum at some subsonic flight condition and then also decreases toward zero. The details of the maximum are, however, not clear from Trilling's work.

As shown by Liepmann and Bryson (reference 10), the slope which the curves of figure 7 should have at the vertical axis can be determined from the previous results regarding the behavior of the local Mach number at the sonic flight condition. For example, taking the derivative of equation (10a) with respect to ξ_0, one can write for the front wedge

$$\left(\frac{d\bar{c}_{d_f}}{d\xi_0}\right)_{\xi_0=0}=2\int_0^{1/2}\left(\frac{d\tilde{C}_p}{d\xi_0}\right)_{\xi_0=0}d\left(\frac{x}{c}\right) \tag{11}$$

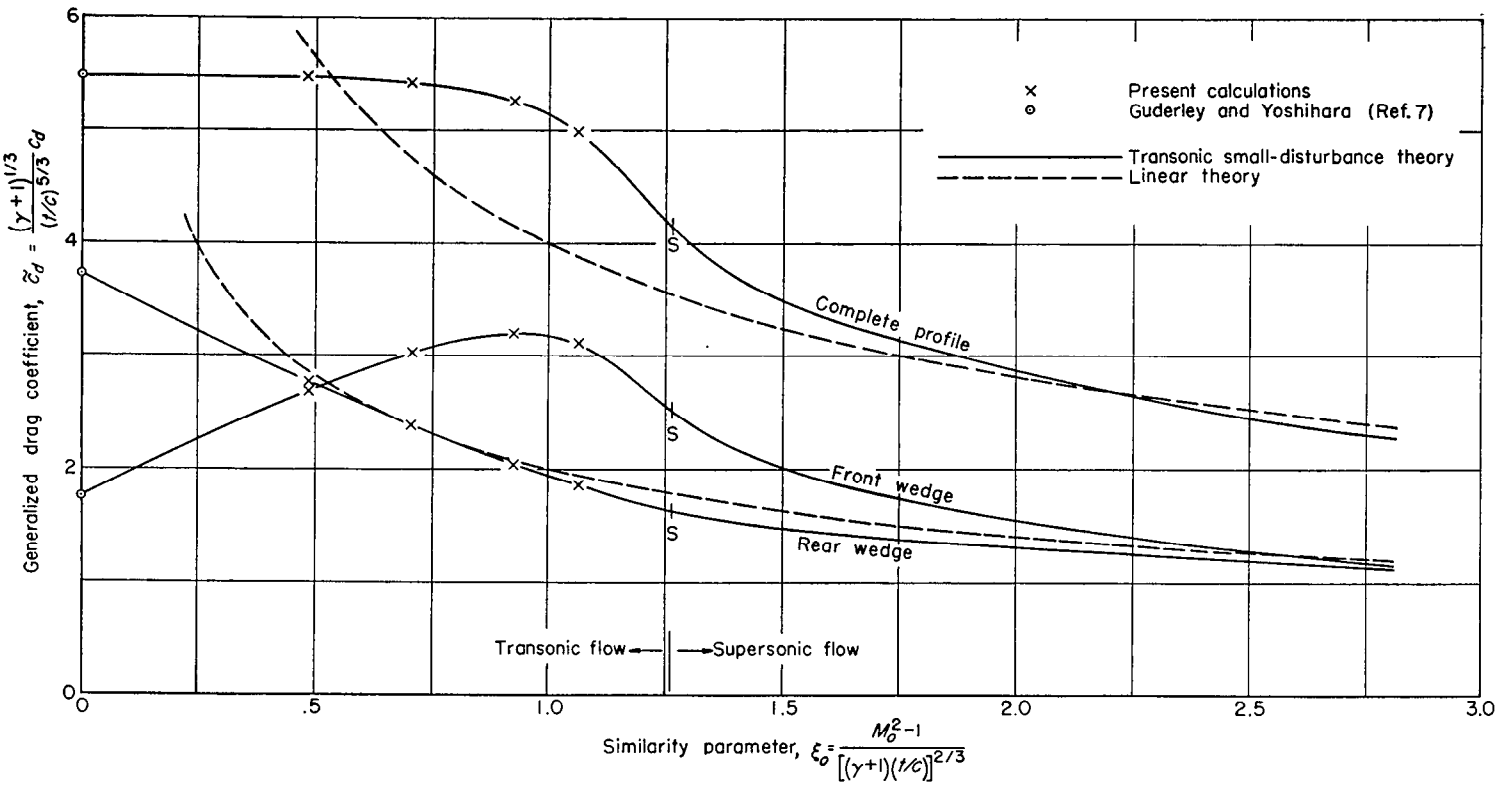

FIGURE 7.—Variation of generalized drag coefficient.

It follows from equation (7) that

$$\left(\frac{d\tilde{C}_p}{d\xi_0}\right)_{\xi_0=0}=-2\left[\left(\frac{d\xi}{d\xi_0}\right)_{\xi_0=0}-1\right]$$

and hence, by virtue of equation (6), that

$$\left(\frac{d\tilde{C}_p}{d\xi_0}\right)_{\xi_0=0}=2$$

Substitution of this value into equation (11) leads to the final result

$$\left(\frac{d\bar{c}_{d_f}}{d\xi_0}\right)_{\xi_0=0}=2 \tag{12a}$$

This is the result given previously by Liepmann and Bryson. The analogous relation for the rear wedge, obtained by proceeding from equation (10b), is

$$\left(\frac{d\bar{c}_{d_r}}{d\xi_0}\right)_{\xi_0=0}=-2 \tag{12b}$$

The curves for the front and rear wedges in figure 7 thus have equal but opposite slopes where they meet the vertical axis. It follows that the curve for the complete profile has zero slope at the same point, that is, $(d\bar{c}_d/d\xi_o)_{\xi_o=o}=0$.

It will be noted that figure 7 also includes curves obtained from the standard linear theory. That such results can be included in a transonic similarity plot of this kind has been shown by several writers (see, for example, reference 22). In the present case, the drag coefficient of the complete profile as given by the linear theory is (see page 154 of reference 23)

$$c_d=4\frac{(t/c)^2}{(M_o^2-1)^{1/2}} \tag{13}$$

This can be written in terms of the transonic similarity variables as

$$\bar{c}_d=\frac{(\gamma+1)^{1/3}}{(t/c)^{5/3}}c_d=\frac{4}{\xi_o^{1/2}} \tag{14}$$

The front and rear of the profile each contribute half of the drag in the linear theory, so that

$$\bar{c}_{d_f}=\bar{c}_{d_r}=\frac{2}{\xi_o^{1/2}}$$

The dashed curves of figure 7 have been drawn in accordance with these relations.

For the rear half of the airfoil, the two theories illustrated in figure 7 are in reasonable agreement down to well within the regime of transonic flow. This result might not be anticipated, since the linear theory is based on the assumption of supersonic flow throughout the flow field. It is probably associated in some way with the fact that the local flow over the entire rear half of the airfoil remains supersonic (and nearly uniform) even after the flow over the front has become subsonic. For the front wedge, the results of the two theories diverge markedly even before the transonic regime is reached. The same is true of the curves for the complete profile. Within the transonic regime itself, the two theories give radically different results for both the front wedge and the complete profile. Near $\xi_o=0$ the two sets of results for the rear wedge are also completely different. This basic disagreement is a reflection of the fact that the linear theory is inherently incapable of dealing with problems involving mixed flows.

To afford some idea of numerical magnitudes for a representative specific case, the curves of figure 7 have been replotted in figure 8 for $t/c=0.0787$ and $\gamma=1.4$. This value of t/c is the value which would apply to a complete profile having the same half-angle at the leading edge (4½°) as the thinnest wedge tested by Liepmann and Bryson (references 8 and 10).[7] Also included in the present figure are partial curves calculated according to the standard shock-expansion method (see, for example, reference 24). This method, which is based on a stepwise application of the complete equations for an oblique shock wave and a Prandtl-Meyer

[7] In an earlier account of this work (see footnote 1), a multiplicity of curves was drawn for each part of the profile on the basis of the transonic small-disturbance theory. This was done by using expressions for the similarity parameter and pressure coefficient different from those of equations (1) and (7). In view of the subsequent developments outlined in footnote 4, such complications now appear to be of lessened significance.

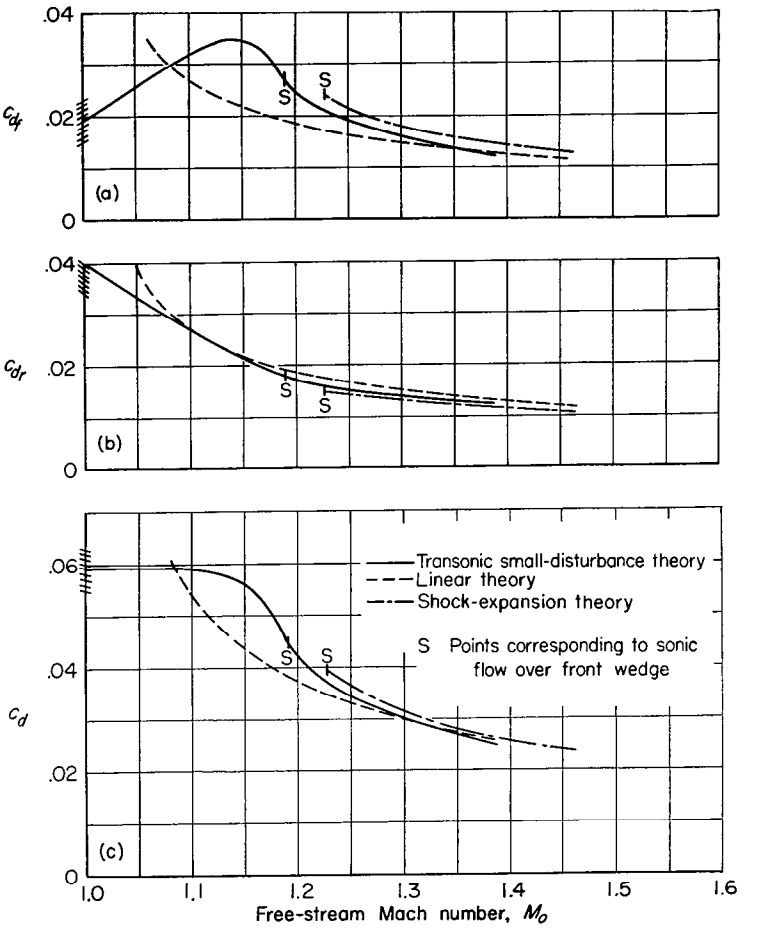

(a) Front wedge.
(b) Rear wedge.
(c) Complete profile.

FIGURE 8.—Variation of drag coefficient with Mach number for $t/c=0.0787$ and $\gamma=1.4$.

expansion, applies only in the range in which the shock-wave equations predict an attached wave with not less than sonic velocity over the front half of the profile. Except for a small error in the drag of the rear half near the low end of this range (see footnote 6), the shock-expansion method provides the exact inviscid solution for the double-wedge profile.

Additional information of an exact nature can be included in figure 8 with reference to the rate of change of the drag coefficient at the sonic flight speed. As previously implied, the analytical results of Guderley regarding flows with a free-stream Mach number close to 1 (reference 19) are not limited by the assumptions of the transonic small-disturbance theory. (The same can also be said of the physical arguments given by Liepmann and Bryson in reference 10.) This means that the result of equation (5)—namely, that $(dM/dM_o)_{M_o=1}=0$—may be regarded as an exact result and may be used to obtain exact relations for the slope of the drag curves at a free-stream Mach number of 1 (see appendix for details). The final equations, which are the only items of importance here, are as follows:

For the front wedge

$$\left(\frac{dc_{d_f}}{dM_o}\right)_{M_o=1}=\frac{4}{\gamma+1}\left(\frac{t}{c}\right)-\frac{2}{\gamma+1}(c_{d_f})_{M_o=1} \tag{16a}$$

For the rear wedge

$$\left(\frac{dc_{d_r}}{dM_o}\right)_{M_o=1}=-\frac{4}{\gamma+1}\left(\frac{t}{c}\right)-\frac{2}{\gamma+1}\,(c_{d_r})_{M_o=1} \qquad (16b)$$

For the complete profile

$$\left(\frac{dc_d}{dM_o}\right)_{M_o=1}=-\frac{2}{\gamma+1}\,(c_d)_{M_o=1} \qquad (16c)$$

The short slanted dashes which appear on the line $M_o=1$ in the various parts of figure 8 have been drawn in accordance with these relations. An exact curve for the transonic range would cross the line $M_o=1$ with a slope conforming with these dashes and fair smoothly into the shock-expansion results at some point slightly to the right of the pertinent point S. The ordinate at $M_o=1$ would not, of course, be necessarily identical with that computed from the small disturbance theory.

It is of interest to compare equations (16) with the corresponding equations given by the small-disturbance theory. These can be found by differentiation of equations (10) and application of the results of equations (12). The final expressions are as follows:

For the front wedge

$$\left(\frac{dc_{d_f}}{dM_o}\right)_{M_o=1}=\frac{4}{\gamma+1}\left(\frac{t}{c}\right) \qquad (17a)$$

For the rear wedge

$$\left(\frac{dc_{d_r}}{dM_o}\right)_{M_o=1}=-\frac{4}{\gamma+1}\left(\frac{t}{c}\right) \qquad (17b)$$

For the complete profile

$$\left(\frac{dc_d}{dM_o}\right)_{M_o=1}=0 \qquad (17c)$$

Equations (17a) and (17b) are the same as equations (16a) and (16b) insofar as the terms proportional to t/c are concerned. These terms are a result (see appendix) of a relative variation between the static pressure at the sonic point and the reference static pressure in the free stream. They have the same magnitude but opposite sign for the front and rear wedges. They thus do not appear in the final equations for the complete profile. Equations (17) differ from the exact equations (16) by their failure in every case to include a negative term proportional to the drag coefficient. This term appears in equations (16) as an effect (see appendix) of a relative variation between the dynamic pressures in the free stream and at the sonic point. This effect is of a higher order than those which the small-disturbance theory includes. Because of the presence of this higher order effect, the exact theoretical curve for the complete profile, in particular, must have a slightly negative slope at a free-stream Mach number of 1.[8]

CONCLUDING REMARKS

The results of the present numerical analysis show the salient features of the two-dimensional inviscid flow over a thin, doubly symmetrical, double-wedge profile in the range of supersonic flight speeds in which the bow wave is detached. The most important findings can be summarized as follows:

1. The vertical extent of the subsonic region behind the detached wave is large even when the wave is only a relatively small distance removed from the leading edge. This implies that the tip effects may be large on finite-span wings when the bow wave is detached.

2. The local Mach number M at a point on the surface of the profile increases monotonically as the free-stream Mach number M_o increases from 1. The increase in M is at first very slight for a considerable increment away from the sonic flight condition. This confirms previous findings that the local Mach number has a stationary value at $M_o=1$ and shows that these findings provide a good working approximation even at Mach numbers a short distance removed from 1. When considered in terms of the pressure coefficient on the surface of the airfoil, the results show how the transonic pressure distribution tends, as the flight Mach number increases, toward the purely supersonic type of distribution known to exist in the upper portion of the speed range.

3. As the free-stream Mach number increases from 1, the pressure-drag coefficient of the front wedge increases until it reaches a maximum at a flight speed somewhat below that for which the bow wave attaches to the leading edge. It then decreases, the rate of the decrease being at first rapid in the vicinity of bow-wave attachment and then less rapid in the range of purely supersonic flow. The drag coefficient of the rear wedge decreases continuously over the entire supersonic range of flight speeds. Because of the differences in the drag variation for the two halves, the drag coefficient of the complete profile varies relatively slightly near the sonic flight speed, decreases rapidly in the vicinity of bow-wave attachment, and then decreases at a progressively less rapid rate in the range of purely supersonic flow.

In applying the foregoing results, it should be remembered that the theory assumes an inviscid fluid and an airfoil of small thickness and infinite span. Since the effects of finite span, in particular, will be to reduce the drag at transonic speeds, the present results should be looked upon as providing an approximate upper bound for the inviscid pressure drag of a three-dimensional wing. In fact, until some knowledge is obtained regarding the effects of finite span and fluid viscosity, it is doubtful if more accurate two-dimensional, inviscid calculations for thin double-wedge profiles would be worth the trouble from an engineering point of view. In the present state of theoretical development, knowledge of these effects will probably have to come from experiment.

[8] This fact was originally pointed out to the authors by Gottfried Guderley.

PART II—DETAILS OF ANALYSIS

The present part of the report is concerned with the details of the numerical analysis. The plan of this part is briefly as follows: In the first section, the basic problem of the finite wedge with detached bow wave is stated as a boundary-value problem for the transonic small-disturbance equation in the hodograph plane. Except for the introduction of a boundary condition along the sonic line to replace conditions previously prescribed in the supersonic portion of the hodograph, this material follows the lines established by Frankl (reference 5) and Guderley (reference 2). It is recounted here primarily for the sake of completeness. In the second section, the boundary-value problem in the hodograph is reduced to a system of finite-difference equations, the solution of which is then obtained by relaxation techniques. This portion of the work, which constitutes the main contribution of the present part of the report, is discussed in some detail, since it is anticipated that the methods and equations which are presented will be useful in the solution of other problems involving detached shock waves. The third section describes the transformation of the hodograph solution for the finite wedge back into the physical plane. The fourth section is concerned with the characteristics construction used to obtain the purely supersonic flow over the rear of the double-wedge profile, and the final section contains a few remarks on the accuracy of the solution.[9]

STATEMENT OF BOUNDARY-VALUE PROBLEM IN HODOGRAPH PLANE

COMPLETE HODOGRAPH

A description of the flow in the physical plane has been given in part I, with figure 1 as the basis for the discussion. For convenience, this figure is reproduced here (with minor changes) as figure 9. The corresponding hodograph of the flow about the front wedge is shown in figure 10. The hodograph variables are the dimensionless speed V/a_* and the inclination of flow θ, where V is the local speed of flow, a_* is the critical speed, and θ is measured relative to the x axis.

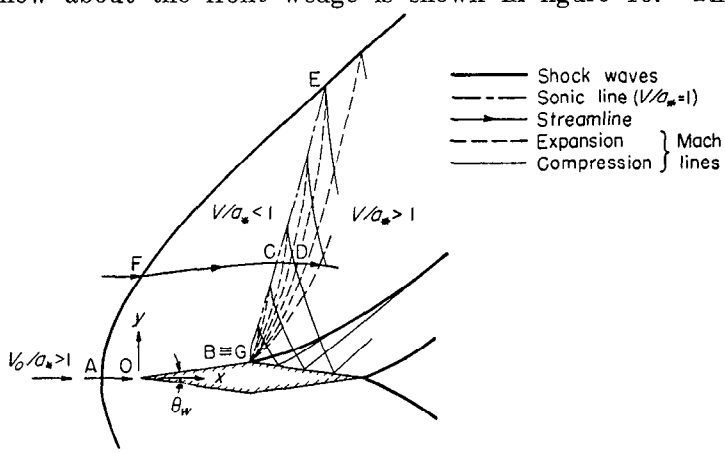

FIGURE 9.—Flow in physical plane.

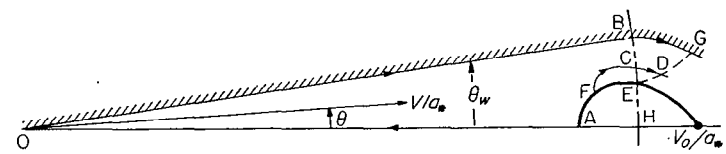

FIGURE 10.—Flow about front wedge in hodograph plane.

The picture in the upper half of the hodograph plane can be described briefly as follows: The part of the shock wave which borders on the subsonic region in the physical plane appears in the hodograph as the subsonic portion AE of a shock polar. The shape and position of the shock polar are determined by the dimensionless free-stream velocity V_0/a_* (or, what is equivalent, by the free-stream Mach number M_0) and by the ratio of specific heats γ.[10] The portion of the central streamline from the normal part of the shock wave to the stagnation point at the nose of the wedge maps into the portion AO of the horizontal axis in the hodograph. The image of the wedge itself is given by a radial line inclined at the wedge angle θ_w and extending from the origin O to the point B on the critical circle ($V/a_*=1$). The shoulder of the wedge, which produces an expansion fan of a locally Prandtl-Meyer type in the physical plane, appears in the hodograph as a portion of the downgoing characteristic (epicycloid) starting at B. The last Mach line from the shoulder to the sonic line (termed the separating Mach line in part I) appears as a portion of the upgoing characteristic which begins at the intersection E of the shock polar and critical circle. Point G, the point of intersection of the epicycloids from B and E, fixes the extent of the downgoing characteristic which must be considered in determining the solution in the hodograph. A typical streamline in the hodograph plane is shown by the line FCD.

To obtain a solution of the detached-wave problem in the hodograph, a boundary-value problem for the differential equations of gas dynamics must be solved within the region AOBGEA. If the stream function ψ is taken as the unknown, the pertinent boundary conditions are as follows:

1. The value of ψ is constant along the basic streamline AOBG.
2. The streamlines (i. e., the lines of constant ψ) leave the shock polar with a direction which is a known function of location on the polar.
3. The increment in ψ over the portion AE of the shock polar has a prescribed value different from zero.

The reason for the first condition is obvious. The second condition is a consequence of the requirement that, at every point on the shock polar, the direction of the shock wave as computed from the solution for ψ must be compatible with the direction given by the equations for an oblique shock wave in a uniform stream. The third condition prevents ψ from being simply a constant throughout the hodograph and, in effect, fixes the scale of the flow field in the physical plane. It will be noted that no condition is prescribed along the boundary EG in the hodograph. Frankl has proved (reference 5) that the solution determined by the foregoing boundary conditions is unique.

[9] The authors are indebted to William A. Mersman of the Ames Laboratory for suggestions leading to certain of the mathematical procedures used in the analysis.

[10] The equations which are pertinent here can be found in the work of Frankl (reference 5).

SPECIALIZATION TO SMALL DISTURBANCES

Original boundary-value problem.—As has been shown by Guderley (reference 2), the equations of the boundary-value problem in the hodograph are considerably simplified when restriction is made to the neighborhood of the critical speed. To this end, the quantity η is introduced according to the relation

$$\eta=(\gamma+1)^{1/3}\frac{V-a_*}{a_*} \tag{18}$$

and η and the stream angle θ are assumed sufficiently small that only their lowest powers need be retained in the analysis. This means, in effect, that the right-hand portion of the previous hodograph (including the shock polar itself) is made to shrink down to the vicinity of the point H, which defines the intersection of the critical circle and the horizontal axis.

When the foregoing procedure is carried out and the limiting process is counteracted by a suitable enlargement of scale, the situation in the small-disturbance hodograph (i. e., in the η, θ plane) appears as in figure 11. Here the critical

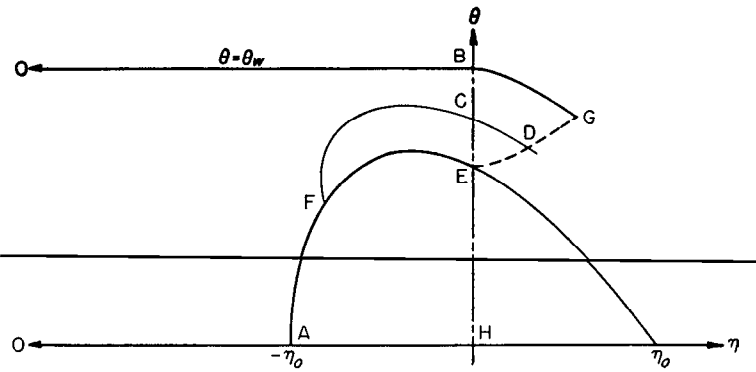

FIGURE 11.—Small-disturbance hodograph.

speed corresponds to the vertical axis $\eta=0$. The equation for the upper half of the shock polar in the simplified hodograph has the form

$$\theta=(\eta_o-\eta)\sqrt{\frac{\eta_o+\eta}{2}} \tag{19}$$

where η_o is the value of η corresponding to the free-stream velocity V_o.[11] By virtue of the limiting process, the stagnation point at 0 has moved, in the present system of axes, infinitely far to the left. As a result, the part AO of the horizontal axis ($\theta=0$) extends now from $\eta=-\eta_o$ to $\eta=-\infty$. The image OB of the wedge is similarly represented by the horizontal line $\theta=\theta_w$, $\eta\leqq 0$. The characteristics, which complete the boundaries of the field, have the simple form

$$\theta=\text{const.}\pm\frac{2}{3}\eta^{3/2} \tag{20}$$

On the basis of the usual assumptions regarding flow near the critical speed, the differential equation for ψ reduces, in the present simplified hodograph, to the form

$$\psi_{\eta\eta}-\eta\psi_{\theta\theta}=0 \tag{21}$$

This is the mixed elliptic-hyperbolic equation studied by Tricomi in reference 13. The boundary conditions along the central streamline require that ψ be constant—say 0—on AO and OBG and that $\psi\to 0$ as $\eta\to(-\infty)$ for $0\leqq\theta\leqq\theta_w$. On the upper half of the shock polar, the boundary conditions require that the lines of constant ψ must have the slope

$$\frac{d\theta}{d\eta}=-\frac{\eta_o+7\eta}{3\eta_o+5\eta}\sqrt{\frac{\eta_o+\eta}{2}} \tag{22a}$$

On a line of constant ψ, $d\theta/d\eta$ can be replaced by $-\psi_\eta/\psi_\theta$ so that the foregoing condition can also be written

$$\psi_\eta-\frac{\eta_o+7\eta}{3\eta_o+5\eta}\sqrt{\frac{\eta_o+\eta}{2}}\,\psi_\theta=0 \tag{22b}$$

The final boundary condition requires that ψ must have some given value $\psi_E\neq 0$ at the point E. Since the coordinates of the flow field will ultimately be expressed in terms of a characteristic dimension of the wedge, the actual value assigned to ψ_E is purely a matter of convenience. As before, no boundary condition is specified along the characteristic EG.

Elimination of the supersonic region.—The foregoing is the boundary-value problem for the finite wedge as formulated by Guderley. It was the original intention in the present work to obtain a numerical solution of this problem on the basis of the boundaries and boundary conditions which have been described. Efforts in this direction failed, however, because of difficulties in obtaining convergence of the relaxation process in the supersonic portion BGE of the hodograph.[12] Similar difficulties have been reported in references 25 and 26 with regard to relaxation calculations of the transonic flow through a converging-diverging nozzle. The reasons for the difficulty in the present case are not apparent. Fundamental questions would appear to be involved concerning the stability and convergence of the finite-difference scheme for the Tricomi equation in the hyperbolic domain. A study of these matters, similar perhaps to that reported for the wave equation in reference 27, may be a prerequisite to numerical solutions of mixed-flow problems in the general case. In the present example, however, the difficulty can be circumvented by modifying the boundary-value problem so as to eliminate the supersonic region from explicit consideration.

The elimination of the supersonic region depends on a formula given by Tricomi (reference 13, equation (2.19)) which relates the behavior of ψ on the vertical axis to its behavior on a characteristic. In the present case, in which ψ is identically zero on the characteristic BG, this formula reduces to an integral relation between ψ and ψ_η at points on the sonic line. This relation has the form

$$F(\lambda)=-k_1\int_0^\lambda\frac{G(\lambda')}{(\lambda-\lambda')^{1/3}}\,d\lambda' \tag{23}$$

where

$$\lambda=\theta_w-\theta$$

$$F(\lambda)=\psi(0,\theta)$$

$$G(\lambda)=\psi_\eta(0,\theta)$$

[11] The derivation of this and the other equations for the simplified hodograph is given by Guderley in reference 5.

[12] Several procedures were tried in the supersonic region, using both a square lattice and a lattice following the characteristics. All were unsuccessful.

and λ' is a variable of integration (see fig. 12). The numerical constant k_1 is given by

$$k_1=\frac{3^{2/3}\Gamma^3(1/3)}{4\pi^2} \tag{24a}$$

where $\Gamma(1/3)$ is the gamma function of the argument 1/3.

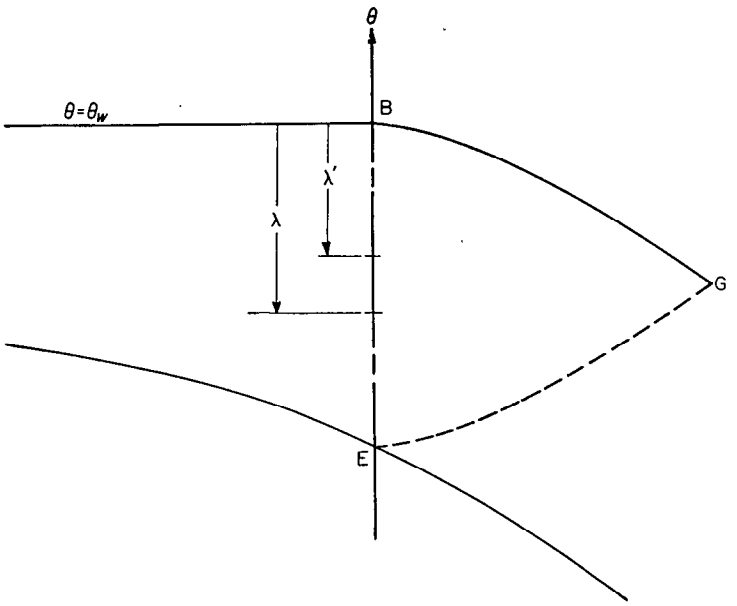

FIGURE 12.—Hodograph in vicinity of sonic line.

For the accuracy required in the later numerical work, the value of this constant may be taken as

$$k_1=1.013 \tag{24b}$$

Satisfying equation (23) everywhere on the sonic line from B to E is completely equivalent to satisfying the condition $\psi=0$ on the downgoing characteristic from B to G.

For the present application, it is convenient to invert equation (23), which can be done by means of Abel's formula. This gives (see reference 28, p. 229)

$$G(\lambda)=-\frac{\sqrt{3}}{2\pi k_1}\frac{d}{d\lambda}\int_0^\lambda \frac{F(\lambda')}{(\lambda-\lambda')^{2/3}}d\lambda'$$

The differentiation indicated on the right is readily accomplished by first transforming the integral to one with fixed limits by means of the substitution $\lambda'=t\lambda$. The result is, after reverting to the original notation,

$$G(\lambda)=-\frac{\sqrt{3}}{2\pi k_1}\frac{1}{\lambda}\left[\frac{1}{3}\int_0^\lambda \frac{F(\lambda')}{(\lambda-\lambda')^{2/3}}\,d\lambda'+\int_0^\lambda \frac{\lambda' F_\lambda(\lambda')}{(\lambda-\lambda')^{2/3}}\,d\lambda'\right]$$

Transforming the first integral through integration by parts and noting that $F(0)=0$, one obtains finally

$$G(\lambda)=-\frac{\sqrt{3}}{2\pi k_1}\int_0^\lambda \frac{F_\lambda(\lambda')}{(\lambda-\lambda')^{2/3}}\,d\lambda'$$

This can be written in the η,θ notation as

$$\psi_\eta(0,\theta)+\frac{\sqrt{3}}{2\pi k_1}\int_{\theta_w}^{\theta}\frac{\psi_\theta(0,\theta')}{(\theta'-\theta)^{2/3}}\,d\theta'=0 \tag{25}$$

where $\theta'=\theta_w-\lambda'$ denotes the variable of integration. As with equation (23), satisfaction of equation (25) everywhere on the sonic line between B and E insures that ψ is zero everywhere on the characteristic from B to G. By regarding equation (25) as a boundary condition along BE, the region of solution of the partial differential equation (21) can be confined to the purely subsonic portion of the hodograph ($\eta\leqq 0$). Relaxation methods can be used to solve the resulting elliptic problem without essential difficulty.

Equations in normalized form.—To carry out the numerical calculations, it is convenient to normalize the equations of the boundary-value problem by means of the transformation

$$\tilde{\eta}=\frac{\eta}{\eta_o},\quad \tilde{\theta}=\sqrt{2}\frac{\theta}{\eta_o^{3/2}} \tag{26}$$

This is equivalent to introducing the rules for transonic similarity (see for example, references 2, 15, and 29). The particular form of transformation chosen here has the advantage for the present work of providing a unique shock polar with conveniently located horizontal and vertical intercepts.

With the foregoing substitution, the differential equation (21) takes on the following form in the $\tilde{\eta},\tilde{\theta}$ plane:

$$\psi_{\tilde{\eta}\tilde{\eta}}-2\tilde{\eta}\,\psi_{\tilde{\theta}\tilde{\theta}}=0 \tag{27}$$

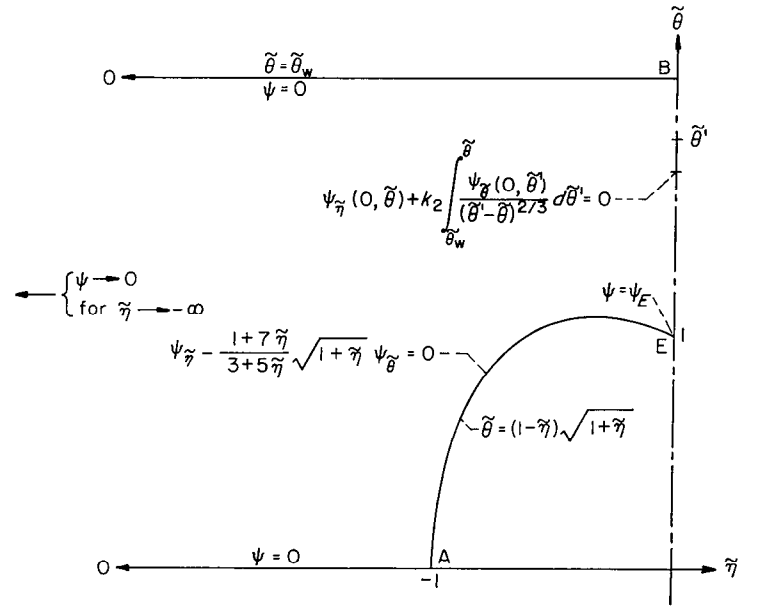

FIGURE 13.—Boundary-value problem in $\tilde{\eta},\tilde{\theta}$ plane.

Consistent with the elimination of the supersonic region, the boundary-value problem can now be summarized as follows (see fig. 13):

1. On the basic streamline AOB:

$$\psi=0 \text{ for } \tilde{\theta}=0,\ \tilde{\eta}\leqq -1 \tag{28}$$

$$\psi=0 \text{ for } \tilde{\theta}=\tilde{\theta}_w,\ \tilde{\eta}\leqq 0 \tag{29}$$

$$\psi\to 0 \text{ for } \tilde{\eta}\to-\infty,\ 0\leqq\tilde{\theta}\leqq\tilde{\theta}_w \tag{30}$$

2. On the shock polar AE:

$$\psi_{\tilde{\eta}}-\frac{1+7\tilde{\eta}}{3+5\tilde{\eta}}\sqrt{1+\tilde{\eta}}\,\psi_{\tilde{\theta}}=0$$

for

$$\tilde{\theta}=(1-\tilde{\eta})\sqrt{1+\tilde{\eta}},\quad -1\leqq\tilde{\eta}\leqq 0 \tag{31}$$

3. On the sonic line BE:

$$\psi_{\tilde{\eta}}(0,\tilde{\theta})+k_2\int_{\tilde{\theta}_w}^{\tilde{\theta}}\frac{\psi_{\tilde{\theta}}(0,\tilde{\theta}')}{(\tilde{\theta}'-\tilde{\theta})^{2/3}}\,d\tilde{\theta}'=0$$

for

$$1\leqq\tilde{\theta}\leqq\tilde{\theta}_w$$

where

$$k_2=\frac{3^{1/2}}{2^{2/3}\pi k_1} \tag{32}$$

4. At the point E:

$$\psi=\psi_E \text{ (arbitrary constant}\neq 0) \text{ for } \tilde{\eta}=0,\tilde{\theta}=1 \tag{33}$$

It is apparent from the preceding equations that a solution of the problem will depend on only the single parameter $\tilde{\theta}_w$, which defines the position of the upper boundary in the $\tilde{\eta},\tilde{\theta}$ plane. This parameter is directly related to the transonic similarity parameter ξ_o which was used in the presentation of the results in part I (see equation (1)). The relation is easily derived with the aid of equations (18) and (26) plus the equation

$$\frac{M^2-1}{(\gamma+1)}=\frac{V}{a_*}-1 \tag{34}$$

which relates the speed and Mach number in the small-disturbance theory. (It is also necessary to note that, to the approximation of the theory, θ_w is equal to t/c.) The final result is

$$\xi_o=\frac{2^{1/3}}{\tilde{\theta}_w{}^{2/3}} \tag{35}$$

SOLUTION OF BOUNDARY-VALUE PROBLEM IN HODOGRAPH PLANE

The solution of the boundary-value problem in the $\tilde{\eta},\tilde{\theta}$ plane is obtained in two steps, according to established procedures for the numerical treatment of partial differential equations. (For introductory articles, see references 30, 31, and 32. For an extended discussion, see reference 33.) In the first step, the domain under consideration is covered by a square lattice, and a finite-difference approximation to the differential equation or boundary condition is written for each lattice point. The boundary-value problem for the partial differential equation is thus reduced to a problem in solving a large number of simultaneous algebraic equations. Solution of the latter problem by relaxation methods is the second step.

REDUCTION TO FINITE-DIFFERENCE EQUATIONS

The arrangement of a typical finite-difference lattice in the $\tilde{\eta},\tilde{\theta}$ plane is shown in figure 14. The basic lattice interval, which is the same in both directions, is denoted by Δ. Adjacent to the shock polar, the interval is adjusted so that the terminal lattice points lie on the polar itself. For purposes of formulating the finite-difference equations, the lattice points are conveniently grouped into five categories as follows (typical points in each category are indicated in the figure):

a. Regular internal points
b. Points far to the left
c. Points adjacent to the shock polar

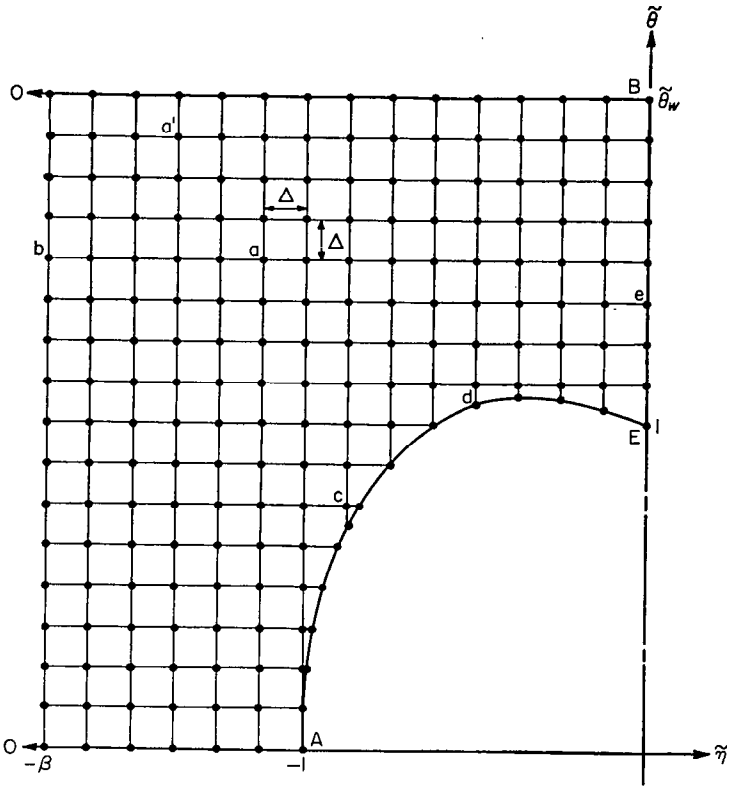

FIGURE 14.—Illustrative finite-difference lattice in the $\tilde{\eta},\tilde{\theta}$ plane.

d. Points on the shock polar
e. Points on the sonic line

The form of the finite-difference equation pertinent to each category will be developed in the following paragraphs. The methods employed are standard, except for the somewhat novel treatment of the boundary conditions along the shock polar and sonic line.

Regular internal points.—The category of regular internal points comprises all points interior to the boundaries but not immediately adjacent to the shock polar. The situation in the vicinity of such a point is as shown in figure 15.

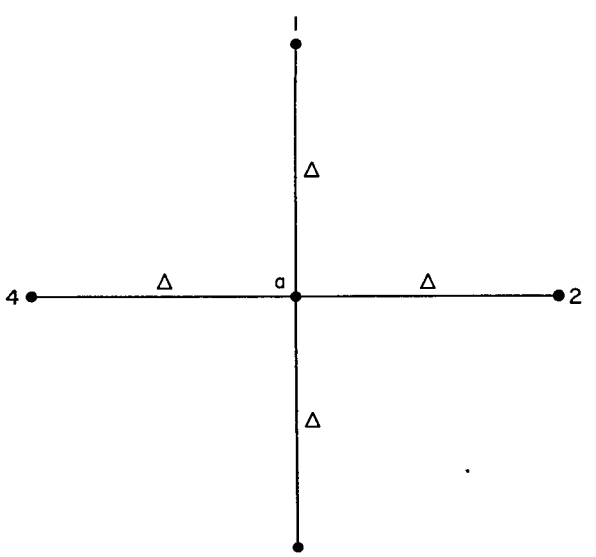

FIGURE 15.—Regular internal point.

The difference equation which applies here is obtained by suitable approximation to the differential equation (27).

If it is assumed that the unknown function $\psi=\psi(\tilde{\eta},\tilde{\theta})$ may be expanded locally in the form of a Taylor's series, the values of ψ at 2 and 4 may be written (see fig. 15)

$$\psi_2=\psi_0+\Delta\psi_{\tilde{\eta}}|_0+\frac{\Delta^2}{2!}\psi_{\tilde{\eta}\tilde{\eta}}|_0+\frac{\Delta^3}{3!}\psi_{\tilde{\eta}\tilde{\eta}\tilde{\eta}}|_0+0(\Delta^4)$$

$$\psi_4=\psi_0-\Delta\psi_{\tilde{\eta}}|_0+\frac{\Delta^2}{2!}\psi_{\tilde{\eta}\tilde{\eta}}|_0-\frac{\Delta^3}{3!}\psi_{\tilde{\eta}\tilde{\eta}\tilde{\eta}}|_0+0(\Delta^4)$$

Addition of these equations and solution for $\psi_{\tilde{\eta}\tilde{\eta}}|_0$ gives

$$\psi_{\tilde{\eta}\tilde{\eta}}|_0=\frac{1}{\Delta^2}(\psi_4-2\psi_0+\psi_2)+0(\Delta^2) \tag{36a}$$

which is a well-known difference expression for the second derivative. The corresponding derivative in the vertical direction is similarly represented by

$$\psi_{\tilde{\theta}\tilde{\theta}}|_0=\frac{1}{\Delta^2}(\psi_3-2\psi_0+\psi_1)+0(\Delta^2) \tag{36b}$$

Substituting these expressions into the differential equation (27) and neglecting the terms $0(\Delta^2)$ then gives for the finite-difference equation at a regular internal point

$$\psi_2+\psi_4-2\tilde{\eta}_0(\psi_1+\psi_3)-2(1-2\tilde{\eta}_0)\psi_0=0 \tag{37}$$

where $\tilde{\eta}_0$ denotes the horizontal coordinate of the point in question. The difference equation for internal points is thus the same for points on a given column but differs from one column to the next. For a point adjacent to the upper boundary OB—as, for example, the point a′ in figure 14—the value of ψ_1 must be set equal to zero in accord with the boundary condition (29). Similar considerations hold for points adjacent to the lower boundary OA.

Equation (37) represents the simplest possible finite-difference approximation to the differential equation (27). As is apparent from the derivation, the error involved is of $0(\Delta^2)$. Consideration has been given to improving the approximation by including additional lattice points in the finite-difference equation or by incorporating higher-order difference corrections in the later relaxation work (c. f., references 34, 35, and 36). Because of the complicated nature of the boundary conditions along the shock polar and sonic line, however, consistent application of these procedures did not appear feasible. The requisite accuracy in the present work has therefore been achieved by suitable decrease in the mesh interval Δ in those regions in which the function ψ varies most rapidly. This procedure has the secondary advantage of providing closely spaced values of the derivatives which are required for the later transformation to the physical plane.

Points far to the left.—In order to carry through the numerical analysis, it is necessary that the finite-difference lattice be terminated at some distance to the left in the hodograph. This can be done with the aid of an asymptotic solution valid for large negative values of $\tilde{\eta}$.

By separation of variables, it can be shown that the general solution of the differential equation (27) in the region $\tilde{\eta}\leqq-1$, $0\leqq\tilde{\theta}\leqq\tilde{\theta}_w$, subject to the boundary conditions (28), (29), and (30), is

$$\psi=\sum_{n=1}^{\infty}A_n\sqrt{-\tilde{\eta}}\sin\left(\frac{n\pi\tilde{\theta}}{\tilde{\theta}_w}\right)K_{1/3}\left[\frac{n\pi}{3\tilde{\theta}_w}(-2\tilde{\eta})^{3/2}\right]$$

where $K_{1/3}$ is the modified Bessel function of the second kind of order ⅓ (notation of reference 37) and A_n is an appropriate constant. At sufficiently large negative values of $\tilde{\eta}$ the first term of the series will predominate, and the above solution can be approximated by

$$\psi=A\sqrt{-\tilde{\eta}}\sin\left(\frac{\pi\tilde{\theta}}{\tilde{\theta}_w}\right)K_{1/3}\left[\frac{\pi}{3\tilde{\theta}_w}(-2\tilde{\eta})^{3/2}\right]$$

If $K_{1/3}$ is then replaced by the first term of its asymptotic expansion (reference 37, p. 202)

$$K_{1/3}(z)\cong\sqrt{\frac{\pi}{2z}}e^{-z}$$

there results finally for ψ the expression

$$\psi=B\sin\left(\frac{\pi\tilde{\theta}}{\tilde{\theta}_w}\right)\times(-\tilde{\eta})^{-1/4}\exp\left[-\frac{\pi}{3\tilde{\theta}_w}(-2\tilde{\eta})^{3/2}\right] \tag{38}$$

where B is an unknown constant.

The asymptotic solution (38) makes it possible to terminate the finite-difference lattice at a position on the left. Consider a typical lattice point in a column located at $\tilde{\eta}=-\beta$ (as, for example, the point b in fig. 14). The neighboring points are then as shown in figure 16, where the

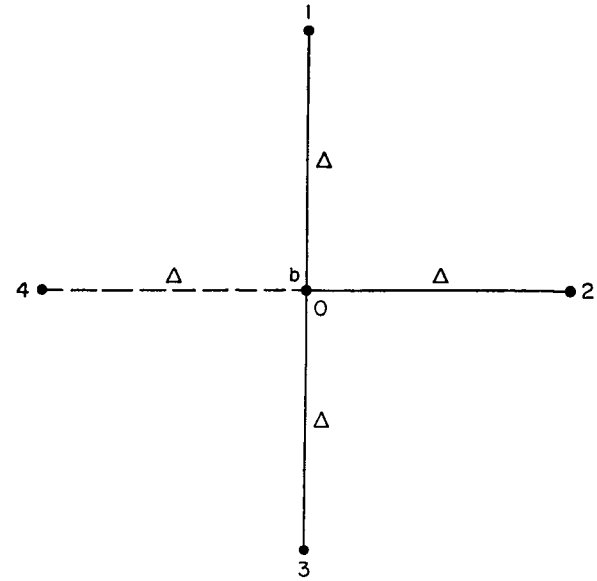

FIGURE 16.—Point at $\tilde{\eta}=-\beta$.

point 4 now represents a fictitious lattice point located at $\tilde{\eta}=-(\beta+\Delta)$. If β is taken sufficiently large that $\Delta/\beta<<1$, then it follows from equation (38) that, to a first order of approximation,

$$\frac{\psi_4}{\psi_0}=\left(1-\frac{\Delta}{4\beta}\right)\exp\left(-\frac{\pi\Delta}{\tilde{\theta}_w}\sqrt{2\beta}\right)$$

Substitution of this value of ψ_4 into the previous equation (37) gives for the finite-difference equation at a point on the left-hand boundary

$$\psi_2+2\beta(\psi_1+\psi_3)+\left[\left(1-\frac{\Delta}{4\beta}\right)\exp\left(-\frac{\pi\Delta}{\tilde{\theta}_w}\sqrt{2\beta}\right)-2(1+2\beta)\right]\psi_0=0 \quad (39)$$

The value of β to be used in any particular case is determined on the basis of computational experience. In general, the larger the value of $\tilde{\theta}_w$, the larger must be the value of β to assure that the use of the asymptotic solution (38) is justified. Since the over-all result is insensitive to changes in the left-hand portion of the field, however, the choice of β is not a critical matter.

Points adjacent to the shock polar.—Points adjacent to the shock polar require special treatment because of the irregularity of the intervals encountered near the curved boundary. Consider the typical case shown in figure 17 (corresponding to point c in fig. 14). Here h and k define the length of the irregular intervals relative to that of the regular interval Δ.

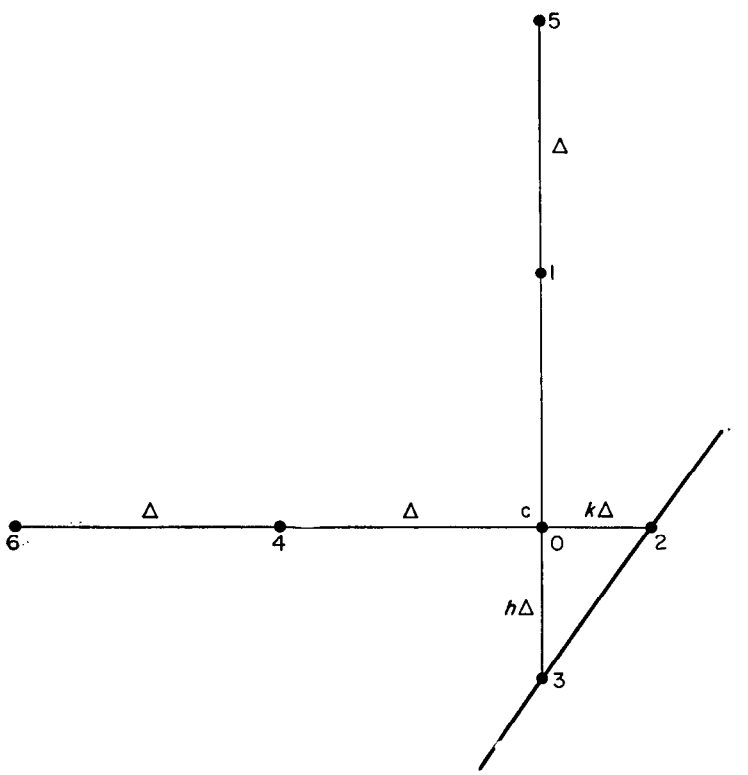

FIGURE 17.—Point adjacent to shock polar.

To obtain the desired accuracy, it was found advisable in the present case to include three rather than two neighboring points in each of the coordinate directions. The value of ψ at the points 2, 4, and 6 is therefore written

$$\psi_2=\psi_0+k\Delta\psi_{\bar{\eta}}|_0+\frac{(k\Delta)^2}{2!}\psi_{\bar{\eta}\bar{\eta}}|_0+\frac{(k\Delta)^3}{3!}\psi_{\bar{\eta}\bar{\eta}\bar{\eta}}|_0+0(\Delta^4)$$

$$\psi_4=\psi_0-\Delta\psi_{\bar{\eta}}|_0+\frac{\Delta^2}{2!}\psi_{\bar{\eta}\bar{\eta}}|_0-\frac{\Delta^3}{3!}\psi_{\bar{\eta}\bar{\eta}\bar{\eta}}|_0+0(\Delta^4)$$

$$\psi_6=\psi_0-2\Delta\psi_{\bar{\eta}}|_0+\frac{(2\Delta)^2}{2!}\psi_{\bar{\eta}\bar{\eta}}|_0-\frac{(2\Delta)^3}{3!}\psi_{\bar{\eta}\bar{\eta}\bar{\eta}}|_0+0(\Delta^4)$$

These may be looked upon as constituting three simultaneous equations for the first three derivatives of ψ in the horizontal direction at the point 0. Solution of these equations for $\psi_{\bar{\eta}\bar{\eta}}|_0$ gives

$$\psi_{\bar{\eta}\bar{\eta}}|_0=\frac{1}{\Delta^2}\left[-\frac{1-k}{2+k}\psi_6+\frac{2(2-k)}{1+k}\psi_4-\frac{3-k}{k}\psi_0+\frac{6}{k(1+k)(2+k)}\psi_2\right]+0(\Delta^2)$$

The corresponding expression for $\psi_{\bar{\zeta}\bar{\zeta}}|_0$ is identical except that k is replaced by h and ψ_2, ψ_4, and ψ_6 by ψ_3, ψ_1, and ψ_5, respectively. Substituting these expressions for the two second derivatives into the differential equation (27) and neglecting terms of $0(\Delta^2)$ then gives for the finite-difference equation at 0

$$\frac{6}{k(1+k)(2+k)}\psi_2+\frac{2(2-k)}{1+k}\psi_4-\frac{1-k}{2+k}\psi_6-2\bar{\eta}_0\left[\frac{6}{h(1+h)(2+h)}\psi_3+\frac{2(2-h)}{1+h}\psi_1-\frac{1-h}{2+h}\psi_5\right]-\left[\frac{3-k}{k}-2\bar{\eta}_0\frac{3-h}{h}\right]\psi_0=0 \quad (40)$$

This reduces to the previous equation (37) when $k=h=1$. (The functions of h and k which appear here have been tabulated in reference 38. The intervals of tabulation are not always sufficiently small, however, to provide the accuracy needed in the present work.)

Points on the shock polar.—In past applications of numerical methods to problems involving curved boundaries, it has not ordinarily been the practice to use a lattice with points located on the boundary itself. The prescribed boundary conditions have then been incorporated in the following manner (cf. references 39 and 40): First, the finite-difference lattice is extended, on the basis of the regular lattice spacing, to include fictitious points external to the boundary. This makes the lattice geometry at internal points adjacent to the boundary the same as at all regular internal points. Next, with the aid of the boundary conditions and suitable interpolation and extrapolation formulas, an expression is obtained for the independent variable at each external point in terms of the values at neighboring internal points. Finally, by substituting these expressions into the finite-difference equation for a regular point, the difference equations are written for the internal points adjacent to the boundary. In this way the boundary conditions are incorporated implicitly into the difference equations at internal points. The procedure is parallel in many respects to that used in terminating the present lattice at the left-hand side of the field.

Although a procedure of the foregoing type can be devised to take care of the boundary conditions on the shock polar, a different approach was found advantageous for the present work. In this approach, the lattice points are placed directly on the boundary as previously described, and a difference equation is obtained at each such point by suitable

finite-difference approximation to the boundary condition. This leads to a somewhat larger system of simultaneous equations than would the more usual procedure but has been found in the long run to give more accurate results with less total effort.

The boundary condition (31), which is thus the basis for the finite-difference equations on the shock polar, can be written

$$\psi_{\tilde{\eta}}-S(\tilde{\eta})\psi_{\tilde{\theta}}=0 \tag{41}$$

where

$$S(\tilde{\eta})=\frac{1+7\tilde{\eta}}{3+5\tilde{\eta}}\sqrt{1+\tilde{\eta}}$$

The problem now is to determine difference expressions for the derivatives $\psi_{\tilde{\eta}}$ and $\psi_{\tilde{\theta}}$ at points on the polar. Consider, for example, the typical situation shown in figure 18 (corresponding to point d of fig. 14). To determine $\psi_{\tilde{\theta}}$, the value

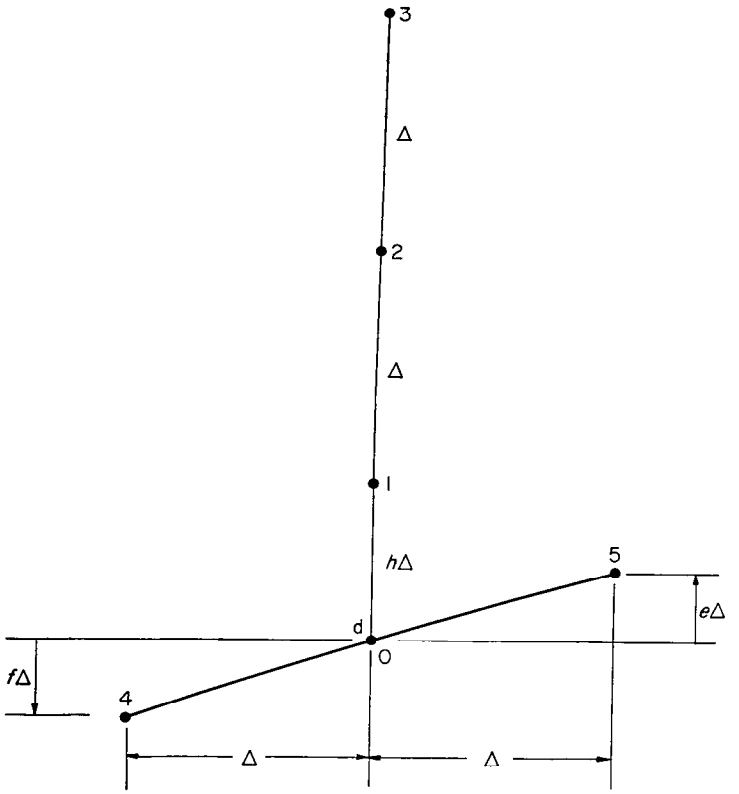

FIGURE 18.—Point on shock polar.

of ψ at each of the interior points 1, 2, and 3 is written, as before, in terms of a Taylor's series about the boundary point 0. Solving the resulting three equations for the derivative $\psi_{\tilde{\theta}}$ at 0 then gives

$$\psi_{\tilde{\theta}}|_0=\frac{1}{\Delta}\left[-\frac{h(2+h)+2(1+h)^2}{h(1+h)(2+h)}\psi_0+\frac{(1+h)(2+h)}{2h}\psi_1-\frac{h(2+h)}{1+h}\psi_2+\frac{h(1+h)}{2(2+h)}\psi_3\right]+0(\Delta^3) \tag{42}$$

This expression, which includes terms of $0(\Delta^2)$, is inconsistent in order of accuracy with the expressions previously employed in setting up the finite-difference equations at internal points. Since end differentiation is, even for a given order of mathematical accuracy, inherently less precise than differentiation at a midpoint (see error terms in reference 38), the retention of the second-order terms was here thought advisable.

The determination of the corresponding expression for $\psi_{\tilde{\eta}}$ is a bit more involved. Expanding ψ at the boundary points 4 and 5 by means of Taylor's series in two dimensions gives

$$\psi_4=\psi_0-\Delta\psi_{\tilde{\eta}}|_0-f\Delta\psi_{\tilde{\theta}}|_0+\frac{\Delta^2}{2!}\psi_{\tilde{\eta}\tilde{\eta}}|_0+f\Delta^2\psi_{\tilde{\eta}\tilde{\theta}}|_0+\frac{(f\Delta)^2}{2!}\psi_{\tilde{\theta}\tilde{\theta}}|_0+0(\Delta^3)$$

$$\psi_5=\psi_0+\Delta\psi_{\tilde{\eta}}|_0+e\Delta\psi_{\tilde{\theta}}|_0+\frac{\Delta^2}{2!}\psi_{\tilde{\eta}\tilde{\eta}}|_0+e\Delta^2\psi_{\tilde{\eta}\tilde{\theta}}|_0+\frac{(e\Delta)^2}{2!}\psi_{\tilde{\theta}\tilde{\theta}}|_0+0(\Delta^3)$$

An expression for $\psi_{\tilde{\theta}}|_0$ is already known from equation (42) in terms of ψ_0, ψ_1, ψ_2, and ψ_3, and an expression for $\psi_{\tilde{\theta}\tilde{\theta}}|_0$ can similarly be determined. The two foregoing expansions may thus be regarded as constituting two equations for the three unknowns $\psi_{\tilde{\eta}}|_0$, $\psi_{\tilde{\eta}\tilde{\eta}}|_0$, and $\psi_{\tilde{\eta}\tilde{\theta}}|_0$. To solve for $\psi_{\tilde{\eta}}|_0$, one more equation is necessary. This is provided by the differential equation (27), which also applies on the boundary and which may be written at the point 0 as

$$\psi_{\tilde{\eta}\tilde{\eta}}|_0-2\tilde{\eta}_0\psi_{\tilde{\theta}\tilde{\theta}}|_0=0$$

The solution for $\psi_{\tilde{\eta}}|_0$ is then found as

$$\psi_{\tilde{\eta}}|_0=\frac{1}{\Delta}\left\{-\frac{e}{e+f}\psi_4-\frac{e-f}{e+f}\psi_0+\frac{f}{e+f}\psi_5-\frac{2ef}{e+f}\psi_{\tilde{\theta}}|_0+\frac{1}{2}\frac{e-f}{e+f}(2\tilde{\eta}_0-ef)\left[\frac{6}{h(2+h)}\psi_0-\frac{3+2h}{h}\psi_1+4\psi_2-\frac{1+2h}{2+h}\psi_3\right]\right\}+0(\Delta^2) \tag{43}$$

where $\psi_{\tilde{\theta}}|_0$ is given by the previous equation (42).[13]

The required finite-difference equation for the point on the shock polar can now be obtained by substituting expressions (42) and (43) into the boundary condition (41) and neglecting the higher-order terms in each case. The result can finally be written

$$\frac{(1+h)(2+h)+2L(3+2h)}{2h}\psi_1-\frac{h(2+h)+4L(1+h)}{1+h}\psi_2+\frac{h(1+h)+2L(1+2h)}{2(2+h)}\psi_3+eK\psi_4-fK\psi_5-\left[\frac{h(2+h)+2(1+h)^2}{h(1+h)(2+h)}+\frac{6L}{h(2+h)}+(e-f)K\right]\psi_0=0 \tag{44}$$

where $K=K(e,f,\tilde{\eta}_o)$ and $L=L(e,f,\tilde{\eta}_o)$ are given by

$$K=\frac{1}{(e+f)S(\tilde{\eta}_0)+2ef}$$

$$L=(e-f)\left(\tilde{\eta}_0-\frac{ef}{2}\right)K$$

Equation (44) is convenient for points on the shock polar for which $-0.6\leq\tilde{\eta}<0$. For $-1<\tilde{\eta}<-0.6$, the general procedure is the same except that the points 0, 1, 2, and 3 are now more conveniently located on a horizontal line and the quantities e, f, and h are redefined accordingly (see fig. 19).

[13] It will be noted that the coefficients in equation (43) become undesirably large as $f\to-e$ and are undefined when $f=-e$. This results from the fact that the determinant of the coefficients in the simultaneous equations used to obtain $\psi_{\tilde{\eta}}|_0$ vanishes when $f=-e$. Difficulties from this source can be avoided by judicious choice of the lattice points.

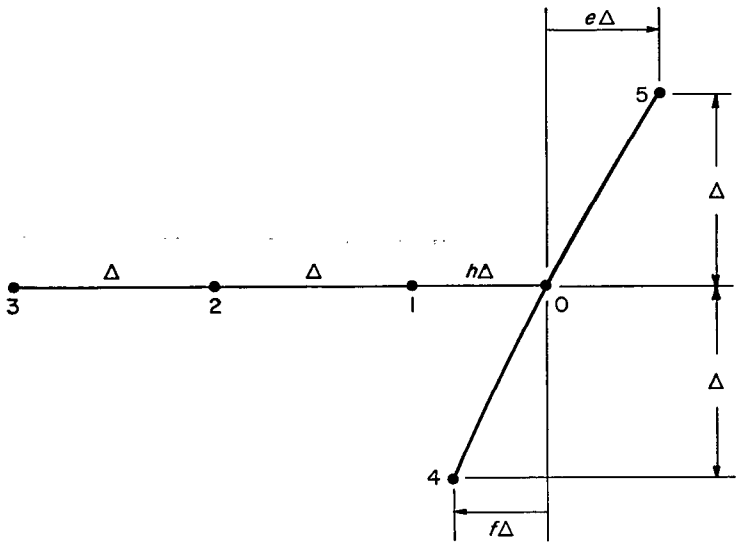

FIGURE 19.—Alternative arrangement for point on shock polar.

The resulting finite-difference equation is identical with equation (44) except that the terms which previously arose from the expression for $\psi_{\tilde{\theta}}|_0$ are now multiplied by -1.

Points on the sonic line.—The difference equation for points on the sonic line is obtained by finite-difference approximation to the boundary condition (32), which can be written, to the accuracy required in the numerical work, as

$$\psi_{\tilde{\eta}}(0,\tilde{\theta})+0.342\int_{\tilde{\theta}_w}^{\tilde{\theta}}\frac{\psi_{\tilde{\theta}}(0,\tilde{\theta}')}{(\tilde{\theta}'-\tilde{\theta})^{2/3}}\,d\tilde{\theta}'=0 \qquad (45)$$

The procedure varies depending on whether the difference equation is being written for the first point below the upper boundary or for one of the lower points.

First point below boundary:

At the first point below the upper boundary the situation is as shown in figure 20. To approximate the integral in

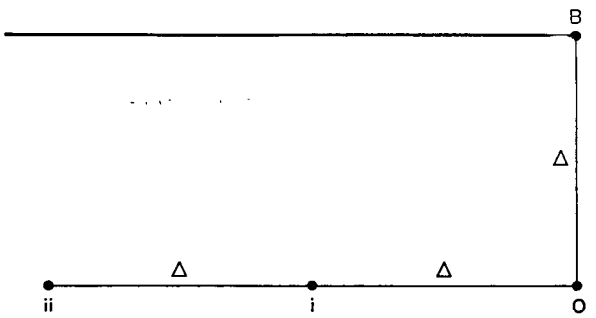

FIGURE 20.—First point on sonic line.

equation (45), use is made of Guderley's singular solution for transonic flow over a convex corner (reference 18). On the basis of this solution, it can be shown that the variation of ψ along the vertical axis in the immediate vicinity of the point B is of the form

$$\psi\sim(\tilde{\theta}_w-\tilde{\theta})^{4/3} \qquad (46)$$

If the lattice spacing is made sufficiently small, this asymptotic relation may be taken as approximately correct over the entire intreval from B to O, so that within this interval

$$\psi=\psi_0\left(\frac{\tilde{\theta}_w-\tilde{\theta}}{\Delta}\right)^{4/3}$$

and

$$\psi_{\tilde{\theta}}=-\frac{4}{3}\,\psi_0\,\frac{(\tilde{\theta}_w-\tilde{\theta})^{1/3}}{\Delta^{4/3}}$$

For the first point below the boundary, the integral in equation (45) can thus be written

$$\int_{\tilde{\theta}_w}^{\tilde{\theta}}\frac{\psi_{\tilde{\theta}}(0,\tilde{\theta}')}{(\tilde{\theta}'-\tilde{\theta})^{2/3}}\,d\tilde{\theta}'=-\frac{4\psi_0}{3\Delta^{4/3}}\int_{\tilde{\theta}_w}^{\tilde{\theta}_w-\Delta}\frac{(\tilde{\theta}_w-\tilde{\theta}')^{1/3}}{[\Delta-(\tilde{\theta}_w-\tilde{\theta}')]^{2/3}}\,d\tilde{\theta}'=\frac{4\psi_0}{3\Delta^{2/3}}\int_0^1\frac{\tau^{1/3}}{(1-\tau)^{2/3}}\,d\tau$$

where $\tau=(\tilde{\theta}_w-\tilde{\theta}')/\Delta$. The integral on the right can be reduced to standard form by means of the substitution $\tau(1-\tau)=z^3/4$, which gives

$$\int_0^1\frac{\tau^{1/3}}{(1-\tau)^{2/3}}\,d\tau=\frac{3}{2^{2/3}}\int_0^1\frac{dz}{\sqrt{1-z^3}}$$

This is an elliptic integral of the first kind. Its value, as determined from the equations and tables of reference 41, is

$$\int_0^1\frac{\tau^{1/3}}{(1-\tau)^{2/3}}\,d\tau=\frac{3}{2^{2/3}}\times\frac{1.846}{3^{1/4}}=2.650$$

The integral in equation (45) thus becomes, in the present case,

$$\int_{\tilde{\theta}_w}^{\tilde{\theta}}\frac{\psi_{\tilde{\theta}}(0,\tilde{\theta}')}{(\tilde{\theta}'-\tilde{\theta})^{2/3}}\,d\tilde{\theta}'=\frac{4}{3}\times2.650\,\frac{\psi_0}{\Delta^{2/3}}=3.533\,\frac{\psi_0}{\Delta^{2/3}} \qquad (47)$$

To approximate the derivative $\psi_{\tilde{\eta}}$ in equation (45), ψ is expanded at points i and ii by means of a Taylor's series about point 0. Terms involving $\psi_{\tilde{\eta}\tilde{\eta}}|_0$ may be omitted here, since the differential equation (27) shows this derivative to be identically zero at points on the sonic line. The values of ψ at i and ii can thus be written

$$\psi_i=\psi_0-\Delta\psi_{\tilde{\eta}}|_0-\frac{\Delta^3}{3!}\,\psi_{\tilde{\eta}\tilde{\eta}\tilde{\eta}}|_0+0(\Delta^4)$$

$$\psi_{ii}=\psi_0-2\Delta\psi_{\tilde{\eta}}|_0-\frac{(2\Delta)^3}{3!}\,\psi_{\tilde{\eta}\tilde{\eta}\tilde{\eta}}|_0+0(\Delta^4)$$

Solution of these equations for $\psi_{\tilde{\eta}}|_0$ gives, to the second order in Δ,

$$\psi_{\tilde{\eta}}|_0=\frac{1}{\Delta}\left(\frac{7}{6}\,\psi_0-\frac{4}{3}\,\psi_i+\frac{1}{6}\,\psi_{ii}\right) \qquad (48)$$

Substitution of expressions (47) and (48) into the boundary condition (45) gives the following finite-difference equation for the first point below the upper boundary:

$$\frac{4}{3}\,\psi_i-\frac{1}{6}\,\psi_{ii}-\left(\frac{7}{6}+1.208\,\Delta^{1/3}\right)\psi_0=0 \qquad (49)$$

Unlike the previous equations (37), (39), (40), and (44) this equation involves the value of Δ.

Lower points:

For a general point below the first lattice point, the situation is as represented in figure 21. The integral in the boundary condition (28) is here evaluated in three sections.

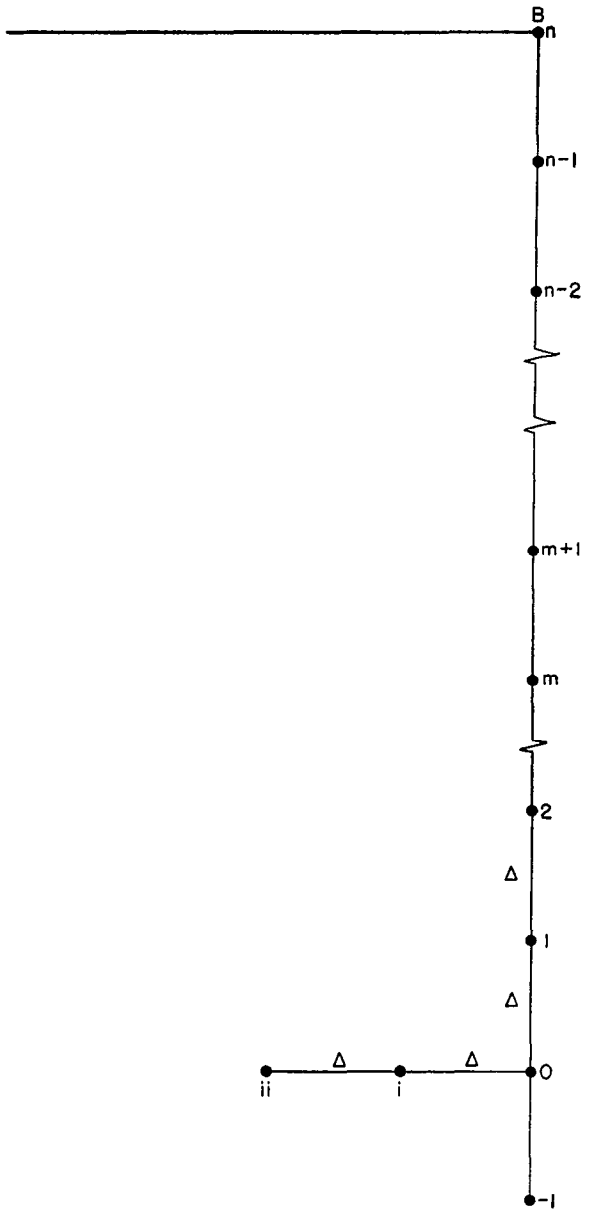

FIGURE 21.—General point on sonic line.

The integral over the lattice interval from B to n-1 is evaluated on the basis of the asymptotic relation used before. The integral from n-1 to 1 is evaluated by assuming a linear variation in ψ over each of the included intervals and then integrating analytically. The linear assumption is sufficiently accurate here, since this entire middle section contributes only a relatively small portion of the complete integral. The integral from 1 to 0, which contains a singularity in the integrand at the point 0, is evaluated by expressing ψ as a cubic in terms of its value at the points 2, 1, 0, and −1 and then integrating analytically as before. The added accuracy of the cubic is required here, since this last section contributes by far the majority of the over-all value. The boundary condition (45) may thus be written

$$\psi_{\tilde{s}}(0,\tilde{\theta})+0.342(J_1+J_2+J_3)=0 \tag{50}$$

where the J's represent the three component integrals just described.

Proceeding to the details of the above procedure, the integral from B to $n-1$ is first written

$$J_1\equiv\int_{\tilde{\theta}_w}^{\tilde{\theta}_w-\Delta}\frac{\psi_{\tilde{s}}(0,\tilde{\theta}')}{[n\Delta-(\tilde{\theta}_w-\tilde{\theta}')]^{2/3}}\,d\tilde{\theta}'=\frac{4\psi_{n-1}}{3\Delta^{2/3}}\int_0^1\frac{\tau^{1/3}}{(n-\tau)^{2/3}}\,d\tau$$

where, as before, $\tau=(\tilde{\theta}_w-\tilde{\theta}')/\Delta$. This integral can be expressed, if desired, as the difference of two elliptic integrals of the first kind. For present purposes, however, it is more convenient (and sufficiently accurate) to expand $(n-\tau)^{-2/3}$ according to the binomial theorem and integrate termwise. This gives finally

$$J_1=\frac{1}{(n\Delta)^{2/3}}\left(1+\frac{8}{21n}+\frac{2}{9n^2}+\frac{160}{1053n^3}+\frac{55}{486n^4}+\cdots\right)\psi_{n-1} \tag{51}$$

This expression is used, of course, only for $n\geqq 2$.

On the basis of the assumption of a linear variation of ψ between adjacent lattice points, the integral from $n-1$ to 1 becomes

$$J_2\equiv\int_{\tilde{\theta}_w-\Delta}^{\tilde{\theta}_w-(n-1)\Delta}\frac{\psi_{\tilde{s}}(0,\tilde{\theta}')}{[n\Delta-(\tilde{\theta}_w-\tilde{\theta}')]^{2/3}}\,d\tilde{\theta}'=\sum_{m=1}^{n-2}\frac{\psi_{m+1}-\psi_m}{\Delta}\int_{\tilde{\theta}_w-(n-m-1)\Delta}^{\tilde{\theta}_w-(n-m)\Delta}\frac{1}{[n\Delta-(\tilde{\theta}_w-\tilde{\theta}')]^{2/3}}\,d\tilde{\theta}'$$

Carrying out the integration gives

$$J_2=\frac{3}{\Delta^{2/3}}\sum_{m=}^{n-2}[(m+1)^{1/3}-m^{1/3}](\psi_m-\psi_{m+1}) \tag{52a}$$

This expression is valid for $n\geqq 3$. (For $n=2$, J_2 obviously does not exist.) For $n>3$ it is convenient to rewrite the summation so that the value of ψ at a given point is not repeated in successive terms of the series. This is done by separating expression (52a) into two series (one with ψ_m and one with ψ_{m+1}), expanding these series, and then regrouping terms. The result is finally

$$J_2=\frac{3}{\Delta^{2/3}}\left\{[2^{1/3}-1]\psi_1+\sum_{m=}^{n-2}[(m+1)^{1/3}-2m^{1/3}+(m-1)^{1/3}]\psi_m-[(n-1)^{1/3}-(n-2)^{1/3}]\psi_{n-1}\right\} \tag{52b}$$

This expression is valid for $n\geqq 4$.

To evaluate the integral from 1 to 0, ψ is represented within this interval by a cubic of the form

$$\psi=a+b\left(\frac{\tilde{\theta}_w-\tilde{\theta}}{\Delta}\right)+c\left(\frac{\tilde{\theta}_w-\tilde{\theta}}{\Delta}\right)^2+d\left(\frac{\tilde{\theta}_w-\tilde{\theta}}{\Delta}\right)^3$$

where a, b, c, and d are determined such that ψ has the proper values at the points 2, 1, 0, and −1. This expression is to be substituted into the integral

$$J_3\equiv\int_{\tilde{\theta}_w-(n-1)\Delta}^{\tilde{\theta}_w-n\Delta}\frac{\psi_{\tilde{s}}(0,\tilde{\theta}')}{[n\Delta-(\tilde{\theta}_w-\tilde{\theta}')]^{2/3}}\,d\tilde{\theta}'$$

The result is finally, after evaluation of the coefficients a, b, c, and d,

$$J_3=\frac{-1}{\Delta^{2/3}}\left(\frac{2}{7}\psi_2-\frac{87}{28}\psi_1+\frac{33}{14}\psi_0+\frac{13}{28}\psi_{-1}\right) \qquad (53)$$

The finite-difference equation for a general point on the sonic line can now be obtained by replacing the J's in equation (50) by the expressions (51), (52), and (53) and using the previous expression (48) for the derivative $\psi_{\tilde{\eta}}|_0$. The result is a lengthy linear equation involving the value of ψ at the points i, ii, -1, 0, 1, 2, . . . , $n-1$, n. Fortunately for the later relaxation work, the coefficients of the terms turn out to be relatively small for all points above the point 2.

Distribution of mesh points.—When an attempt is made to solve the present problem with a coarse mesh, it is soon found that most of the variation in ψ takes place in a relatively small region near the intersection of the shock polar and sonic line. To obtain a sufficiently accurate solution in a practicable length of time, it is therefore necessary to employ a graded lattice, that is, a lattice which has different spacing in different parts of the field. Figure 22 shows the distribution of lattice spacing found satisfactory in a typical case ($\tilde{\theta}_w=1.6$). The particular arrangement shown here involves

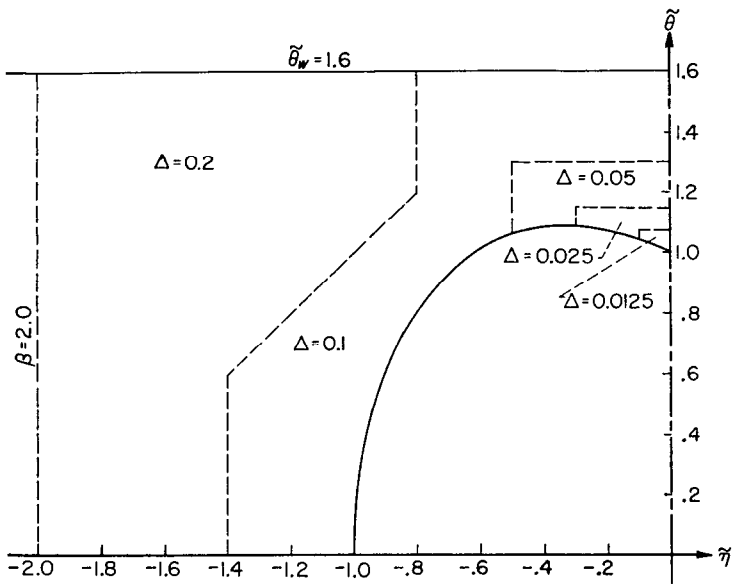

FIGURE 22.—Distribution of lattice spacing for $\tilde{\theta}_w=1.6$.

a total of 228 lattice points. For other values of $\tilde{\theta}_w$, the grading of the lattice follows the same general scheme. Obviously, however, the total number of lattice points must be increased as the upper boundary is moved farther from the shock polar.[14]

Formulas (51), (52), and (53), which are used to approximate the integral along the sonic line, presume the existence of lattice points at a uniform interval over the full distance from the upper boundary to the point in question. This condition is not fulfilled in a graded lattice such as that indicated in figure 22. Some modification of the method must therefore be made to obtain the finite-difference equation for a point on the sonic line in one of the regions of finer mesh. This requirement was satisfied by means of a simple averaging process in which the contribution of nonexistent fine-mesh points is replaced by an average contribution expressed in terms of ψ at bracketing points on the available coarser net. Since the contribution of individual points is small even for points only moderately removed from that at which the equation applies, a rather crude averaging process is sufficient in most cases. (The details need not be given here as they would soon become apparent to anyone working with the method.) When the averaging procedure would not be sufficiently accurate (as when the point at which the equation applies is near the line of demarcation between two different sized meshes), fictitious intermediate points are introduced into the coarser net and the value of ψ at these points is obtained from plots of the distribution of ψ along the sonic line.

SOLUTION OF FINITE-DIFFERENCE EQUATIONS

By the methods of the foregoing section, a finite-difference equation can be obtained for each lattice point in the hodograph plane. The result is a large number of simultaneous algebraic equations involving an equal number of unknown values of ψ. Since the number of unknowns in each equation is small, the equations lend themselves well to solution by relaxation techniques.[15]

The mechanics of the relaxation process have been well described by various authors (references 30, 31, 32, and 33) and need not be gone into here. For present purposes it was found satisfactory to take ψ_E in the boundary condition (33) equal to 10,000 and work with integer values of ψ throughout most of the field. The residuals in the relaxation process were eliminated to within limits of ± 2 (with due care, of course, that all residuals in any given area were not predominately of the same sign). To obtain satisfactory smoothness of the solution near the left-hand boundary in some examples, it was necessary in this region to work with values of ψ to 0.1 and eliminate residuals to within ± 0.5. Whenever the coefficients in the finite-difference equations were relatively small, the corresponding terms were neglected in the point-by-point adjustment of ψ. The error so introduced was eliminated periodically by recomputing the residuals using all terms in the finite-difference equations. This procedure was particularly helpful in the case of the lengthy equations which apply at points on the sonic line. The transition between the various regions of the graded lattice, which is not often discussed in the literature, was accomplished by the use of overlapping fields in essentially the manner described in reference 42.

By means of the foregoing procedures, the boundary-value problem in the hodograph plane has been solved for values of $\tilde{\theta}_w$ of 1.3, 1.6, 2.4, and 4.2. These are equivalent, respectively (see equation (35)), to values of ξ_o of 1.058, 0.921, 0.703, and 0.484 as given previously in part I. As an example of the solution in the hodograph plane, the variation of ψ for $\tilde{\theta}_w=1.6$ is shown as a function of $\tilde{\eta}$ and $\tilde{\theta}$ in figure 23.

[14] Occasionally, when two points on or adjacent to the shock polar fall very close together, one of the points is arbitrarily omitted. An expression for the omitted value of ψ, which is then necessary to complete the difference equation at neighboring points, is found by parabolic interpolation between the values at the available locations.

[15] It is interesting to note that, of the complete set of simultaneous equations, only two—those for the points on the shock polar and sonic line immediately adjacent to the point E—are not homogeneous. Only this fact prevents the solution of the complete set from being identically zero.

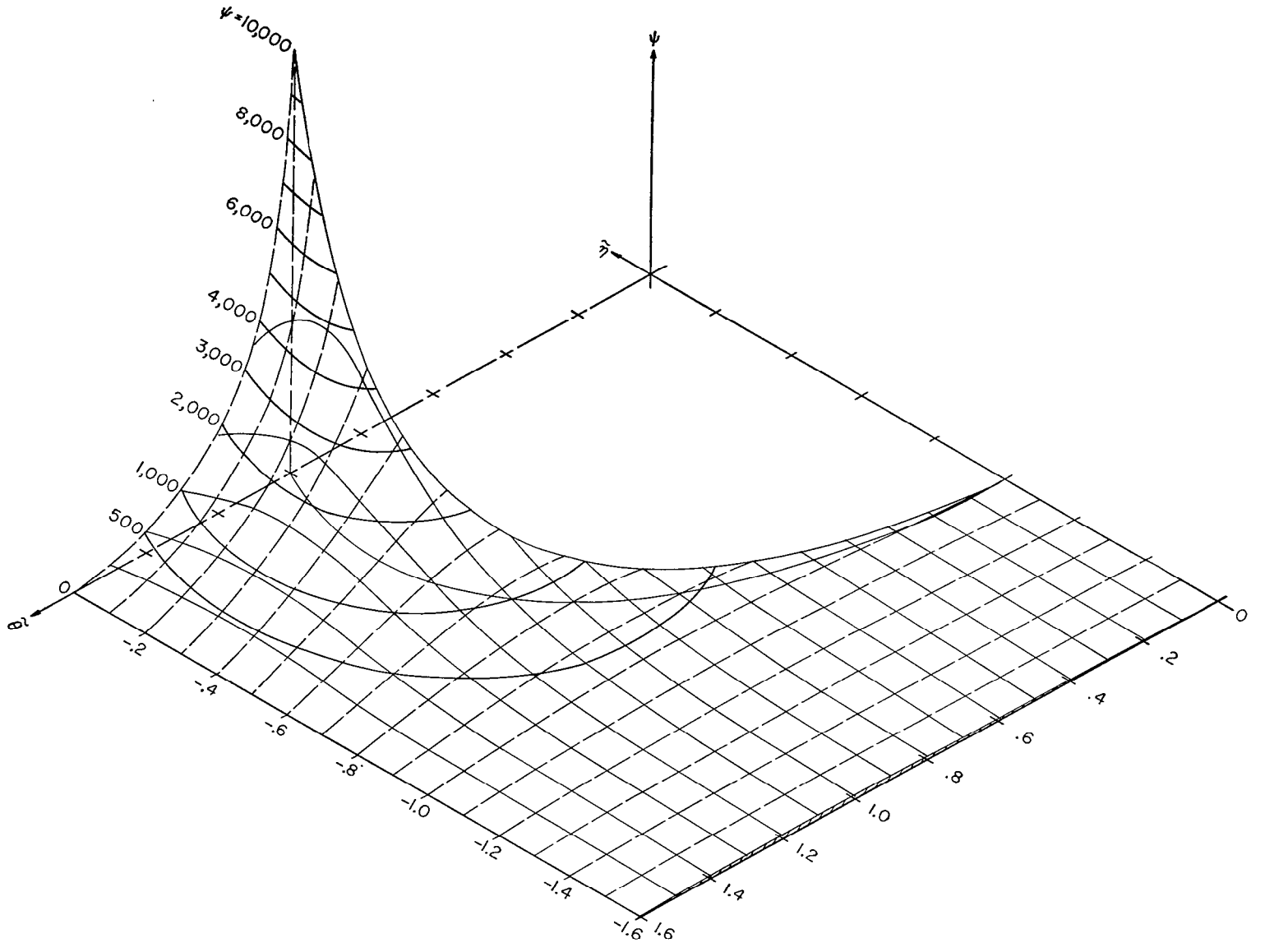

FIGURE 23.—Representation of ψ as a function of $\bar{\eta}$ and $\tilde{\theta}$ for $\tilde{\theta}_w=1.6$ ($\xi_0=0.921$).

(These results correspond to the results shown in the physical plane in fig. 3.) Figure 23 shows clearly the rapid variation of ψ near the intersection of the shock polar and sonic line. The calculated values of ψ corresponding to figure 23 are listed in table I at the end of the report.

TRANSFORMATION TO PHYSICAL PLANE

FLOW FIELD

The transformation from the hodograph plane to the physical plane is governed, in the small-disturbance theory, by the following equations (cf. reference 2):

$$dx=\frac{(\gamma+1)^{1/3}}{\rho_* a_*}(\eta\psi_\theta d\eta+\psi_\eta d\theta)$$

$$dy=\frac{1}{\rho_* a_*}(\psi_\eta d\eta+\psi_\theta d\theta)=\frac{1}{\rho_* a_*}d\psi$$

the second of these equations implies that, in a flow field determined according to the transonic small-disturbance theory, all streamlines appear as straight lines parallel to the horizontal axis. When expressed in terms of $\bar{\eta}$ and $\tilde{\theta}$ the foregoing equations become

$$dx=\frac{(\gamma+1)^{1/3}}{\rho_* a_*}\sqrt{\frac{\eta_o}{2}}(2\bar{\eta}\psi_{\tilde{\theta}}d\bar{\eta}+\psi_{\bar{\eta}}d\tilde{\theta})$$

$$dy=\frac{1}{\rho_* a_*}(\psi_{\bar{\eta}}d\bar{\eta}+\psi_{\tilde{\theta}}d\tilde{\theta})=\frac{1}{\rho_* a_*}d\psi$$

The length l of the wedge, which is equal to one-half the chord of the double-wedge profile, can be found by integrating the first of these equatons over the upper boundary OB of the hodograph (see fig. 24). This gives

$$l=\frac{c}{2}=\frac{(\gamma+1)^{1/3}}{\rho_* a_*}\sqrt{\frac{\eta_o}{2}}\times 2\int_{-\infty}^{0}\bar{\eta}\psi_{\tilde{\theta}}(\bar{\eta},\tilde{\theta}_w)d\bar{\eta}$$

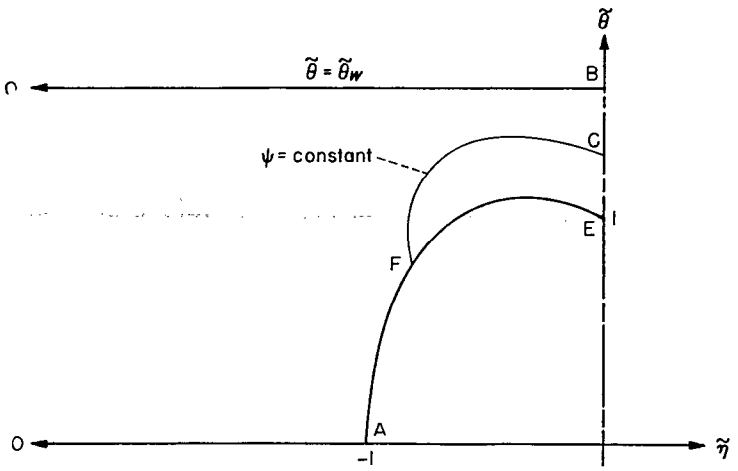

FIGURE 24.—Small-disturbance hodograph in normalized form.

With this relation the previous transformation equations can be put in the dimensionless form

$$d\left(\frac{x}{c}\right)=\frac{1}{4I_w}\left(2\tilde{\eta}\psi_{\tilde{\theta}}d\tilde{\eta}+\psi_{\tilde{\eta}}d\tilde{\theta}\right) \tag{54}$$

$$(\gamma+1)^{1/3}\sqrt{\frac{\eta_o}{2}}\,d\left(\frac{y}{c}\right)=\frac{1}{4I_w}\,d\psi \tag{55}$$

where I_w represents the integral

$$I_w=\int_{-\infty}^{0}\tilde{\eta}\psi_{\tilde{\theta}}(\tilde{\eta},\tilde{\theta}_w)\,d\tilde{\eta} \tag{56}$$

To obtain the flow field in the form given in part I, equation (55) must be rewritten in terms of the ordinate function Y (see equation (2)). The result, derived with the aid of the relation

$$\tilde{\theta}_w=\sqrt{2}\,\frac{t/c}{\eta_o^{2/3}}$$

is

$$dY=[(\gamma+1)(t/c)]^{1/3}\,d\left(\frac{y}{c}\right)=\frac{(2\tilde{\theta}_w)^{1/3}}{4I_w}\,d\psi \tag{57a}$$

Integrating this relation, subject to the condition that $Y=0$ when $\psi=0$, gives

$$Y=[(\gamma+1)(t/c)]^{1/3}\left(\frac{y}{c}\right)=\frac{(2\tilde{\theta}_w)^{1/3}}{4I_w}\,\psi \tag{57b}$$

To utilize the foregoing equations for actual computations, it is first necessary to evaluate I_w. Since numerical values of ψ are available in the hodograph only for $-\beta\leqq\tilde{\eta}\leqq 0$, the evaluation must be caried out in two parts as follows:

$$I_w=\int_{-\beta}^{0}\tilde{\eta}\psi_{\tilde{\theta}}(\tilde{\eta},\tilde{\theta}_w)\,d\tilde{\eta}+\int_{-\infty}^{-\beta}\tilde{\eta}\psi_{\tilde{\theta}}(\tilde{\eta},\tilde{\theta}_w)\,d\tilde{\eta} \tag{58}$$

The first integral is evaluated from the results of the numerical solution by mechanical integration of a curve of $\tilde{\eta}\psi_{\tilde{\theta}}(\tilde{\eta},\tilde{\theta}_w)$ versus $\tilde{\eta}$. The values of the derivative used for this purpose are obtained from the equation

$$\psi_{\tilde{\theta}}|_0=\frac{1}{\Delta}\left(-\frac{4}{3}\psi_1+\frac{1}{6}\psi_2\right) \tag{59}$$

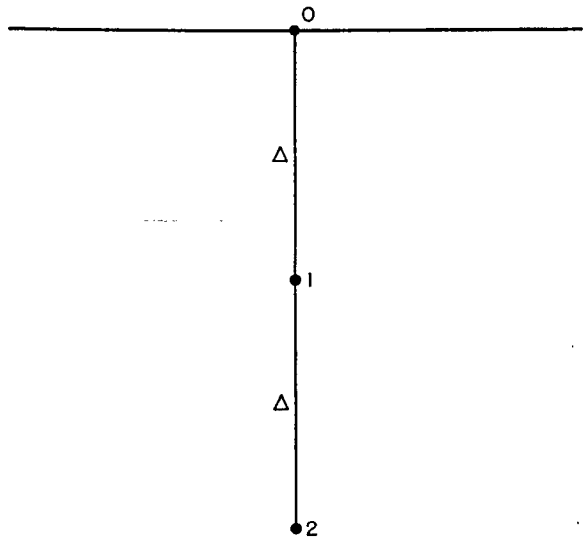

FIGURE 25.—Point on upper boundary.

where the notation is as shown in figure 25. This equation is derived in the same way as equation (48), except that ψ_0 is here taken equal to zero in accord with the boundary condition.[16] It can be shown from Guderley's singular solution for corner flow that for small negative values of $\tilde{\eta}$ the curve of $\tilde{\eta}\psi_{\tilde{\theta}}(\tilde{\eta},\tilde{\theta}_w)$ must behave essentially as $|\tilde{\eta}|^{3/2}$. This result is useful in fairing the numerical results near $\tilde{\eta}=0$. The first integral in equation (58) contributes by far the majority (about 99 percent) of the total value of I_w.

To evaluate the second integral in equation (58) use is again made of the asymptotic solution (38). For this purpose, the constant B is determined such that the value of $\psi_{\tilde{\theta}}$ given by the asymptotic solution matches the numerically determined value at the point $(-\beta,\tilde{\theta}_w)$. Substitution of equation (38) into the second integral of equation (58) then gives

$$\int_{-\infty}^{-\beta}\tilde{\eta}\psi_{\tilde{\theta}}(\tilde{\eta},\tilde{\theta}_w)d\tilde{\eta}=-\frac{\beta^{1/4}\psi_{\tilde{\theta}}(-\beta,\tilde{\theta}_w)}{\exp\left[-\frac{\pi}{3\tilde{\theta}_w}(2\beta)^{3/2}\right]}\times$$

$$\int_{-\infty}^{-\beta}(-\tilde{\eta})^{3/4}\exp\left[-\frac{\pi}{3\tilde{\theta}_w}(-2\tilde{\eta})^{3/2}\right]d\tilde{\eta} \tag{60}$$

where $\psi_{\tilde{\theta}}(-\beta,\tilde{\theta}_w)$ is determined from equation (59) applied at $\tilde{\eta}=-\beta$. The integral on the right is transformed through the substitution

$$\frac{\pi}{3\tilde{\theta}_w}(-2\tilde{\eta})^{3/2}=\omega$$

which gives

$$\int_{-\infty}^{-\beta}(-\tilde{\eta})^{3/4}\exp\left[-\frac{\pi}{3\tilde{\theta}_w}(-2\tilde{\eta})^{3/2}\right]d\tilde{\eta}=$$

$$\frac{1}{3\times 2^{3/4}}\left(\frac{3\tilde{\theta}_w}{\pi}\right)^{7/6}\int_{\frac{\pi}{3\tilde{\theta}_w}(2\beta)^{3/2}}^{\infty}\omega^{1/6}e^{-\omega}d\omega$$

[16] The fact that the second derivative $\psi_{\tilde{\theta}\tilde{\theta}}|_0$ may be taken as zero in the present derivation follows from the boundary condition and the differential equation (10).

The integral here is then found with sufficient accuracy by means of the following asymptotic formula, valid for large values of the lower limit (see pp. 95–96 of reference 43):

$$\int_z^\infty \omega^{\nu-1}e^{-\omega}d\omega \cong z^{\nu-1}e^{-z}$$

Equation (60) thus reduces finally to

$$\int_{-\infty}^{-\beta} \tilde{\eta}\psi_{\tilde{\theta}}(\tilde{\eta},\tilde{\theta}_w)d\tilde{\eta} = -\left(\frac{\beta}{2}\right)^{1/2}\frac{\tilde{\theta}_w}{\pi}\psi_{\tilde{\theta}}(-\beta,\tilde{\theta}_w) \tag{61}$$

With the value of I_w known, equations (54) and (57) can be used to obtain the coordinates x/c and Y corresponding to any point in the $\tilde{\eta},\tilde{\theta}$ plane. The value of Y is obtained by direct substitution of the appropriate value of ψ into equation (57b). The value of x/c must be found by suitable integration of equation (54). The location of the vertex A of the shock wave is found, for example, by integrating equation (54) along the line OA in the hodograph (see fig. 24). If the leading edge 0 is taken as the origin in the physical plane, this gives

$$\left(\frac{x}{c}\right)_A = \frac{1}{2I_w}\int_{-\infty}^{-1} \tilde{\eta}\psi_{\tilde{\theta}}(\tilde{\eta},0)d\tilde{\eta} \tag{62}$$

The integral here is evaluated in two parts following the procedure previously used in determining I_w.

For the abscissa of a point F on the shock wave, equation (54) gives

$$\left(\frac{x}{c}\right)_F = \left(\frac{x}{c}\right)_A + \frac{1}{4I_w}\int_A^F (2\tilde{\eta}\psi_{\tilde{\theta}}d\tilde{\eta}+\psi_{\tilde{\eta}}d\tilde{\theta})$$

where the integration is now taken from A to F along the shock polar. For purposes of numerical evaluation, the integrand here can be simplified by writing

$$2\tilde{\eta}\psi_{\tilde{\theta}}d\tilde{\eta}+\psi_{\tilde{\eta}}d\tilde{\theta} = \frac{2\tilde{\eta}\psi_{\tilde{\theta}}d\tilde{\eta}+\psi_{\tilde{\eta}}d\tilde{\theta}}{\psi_{\tilde{\eta}}d\tilde{\eta}+\psi_{\tilde{\theta}}d\tilde{\theta}}\,d\psi = \frac{2\tilde{\eta}+(\psi_{\tilde{\eta}}/\psi_{\tilde{\theta}})(d\tilde{\theta}/d\tilde{\eta})}{(\psi_{\tilde{\eta}}/\psi_{\tilde{\theta}})+(d\tilde{\theta}/d\tilde{\eta})}\,d\psi$$

If $(\psi_{\tilde{\eta}}/\psi_{\tilde{\theta}})$ and $(d\tilde{\theta}/d\tilde{\eta})$ are replaced by the appropriate functions of $\tilde{\eta}$ from equations (31), there results finally

$$\left(\frac{x}{c}\right)_F = \left(\frac{x}{c}\right)_A + \frac{1}{4I_w}\int_0^{\psi_F}\sqrt{1+\tilde{\eta}}\,d\psi \tag{63}$$

The integral in this equation is evaluated by plotting a curve of ψ versus $\sqrt{1+\tilde{\eta}}$ from the numerical results along the shock polar and carrying out the necessary integration by mechanical means.

The abscissa of a point on the sonic line is found by integrating equation (54) along the $\tilde{\theta}$ axis from B to C. Since point B is situated in the physical plane at $x/c=\frac{1}{2}$, this gives

$$\left(\frac{x}{c}\right)_C = \frac{1}{2}+\frac{1}{4I_w}\int_{\tilde{\theta}_w}^{\tilde{\theta}_C}\psi_{\tilde{\eta}}(0,\tilde{\theta})d\tilde{\theta} \tag{64}$$

The integral here is evaluated by mechanical integration of a curve of $\psi_{\tilde{\eta}}(0,\tilde{\theta})$ versus $\tilde{\theta}$, where $\psi_{\tilde{\eta}}(0,\tilde{\theta})$ is found from equation (48). As can be seen from equation (45) and relation (46), $\psi_{\tilde{\eta}}(0,\tilde{\theta})$ in the vicinity of point B varies essentially as $(\tilde{\theta}_w-\tilde{\theta})^{2/3}$. This fact is of use in drawing the curve of $\psi_{\tilde{\eta}}(0,\tilde{\theta})$ near $\tilde{\theta}=\tilde{\theta}_w$. It can further be seen with the aid of equation (57b) that near the shoulder of the wedge the transformed sonic line has the form

$$\left(\frac{x}{c}\right)_C - \frac{1}{2} \sim Y^{5/4}$$

This relation is useful in establishing the detailed shape of the sonic line in the physical plane. It shows, in particular, that the sonic line will have a vertical tangent and an infinite curvature at the shoulder of the wedge.

PRESSURE DISTRIBUTION AND DRAG

To complete the analysis of the front wedge, it is left to determine the pressure distribution and drag. Integration of equation (54) gives for the chordwise location on the wedge of a given value of $\tilde{\eta}$

$$\frac{x}{c} = \frac{1}{2I_w}\int_{-\infty}^{\tilde{\eta}} \tilde{\eta}\psi_{\tilde{\theta}}(\tilde{\eta},\tilde{\theta}_w)d\tilde{\eta}$$

or

$$\frac{x}{c} = \frac{1}{2}+\frac{1}{2I_w}\int_0^{\tilde{\eta}} \tilde{\eta}\psi_{\tilde{\theta}}(\tilde{\eta},\tilde{\theta}_w)d\tilde{\eta} \tag{65}$$

The speed parameter $\xi=(M^2-1)/[(\gamma+1)(t/c)]^{2/3}$, which was used to present the results in part I, is related to $\tilde{\eta}$ by the following equation, derived with the aid of equations (18), (26), (34), and (35):

$$\xi = \xi_o\tilde{\eta} = \frac{2^{1/3}}{\tilde{\theta}_w^{2/3}}\tilde{\eta} \tag{66}$$

With these equations, the distribution of ξ as a function of x/c is readily determined. The integration of equation (65) is carried out by mechanical means using the same curve previously employed to determine I_w. To fair the resulting ξ curve in the vicinity of the shoulder, use is again made of Guderley's analytical findings, which show that in this vicinity

$$\xi \sim \left(\frac{1}{2}-\frac{x}{c}\right)^{2/5}$$

With the chordwise distribution of ξ known, the pressure distribution and drag can be found as described in part I (see equations (7), (8), and (10)).[17]

CHARACTERISTICS CONSTRUCTION OVER REAR OF AIRFOIL

The characteristics in the $\tilde{\eta}$, $\tilde{\theta}$ plane ($\tilde{\eta}>0$) are given by the following relation obtained from equations (20) and (26):

$$\tilde{\theta} = \text{const.} \pm \frac{2^{3/2}}{3}\tilde{\eta}^{3/2} \tag{67}$$

The corresponding directions of the Mach lines in the generalized physical plane, as determined from this relation and the transformation equations (54) and (57a), are

$$\frac{dY}{d(x/c)} = \pm\frac{(2\tilde{\theta}_w)^{1/3}}{(2\tilde{\eta})^{1/2}} \tag{68}$$

To the present order of approximation, therefore, the slope of the Mach lines is independent of the local inclination $\tilde{\theta}$.

[17] The analytical allowance for the singularity at the leading edge, mentioned in connection with equation (10b), is easily found with the aid of the asymptotic solution (38).

This is consistent with the previous result that the streamlines must appear in the physical plane as horizontal straight lines. As a consequence, the construction of the Mach net over the rear of the airfoil is particularly simple in the small-disturbance theory.

To aid in the construction, the equations for the characteristics in the $\tilde{\eta}, \tilde{\theta}$ plane can be conveniently written in the form

$$\tilde{\theta}=\tilde{\Theta}_u+\frac{2^{3/2}}{3}\tilde{\eta}^{3/2}$$

$$\tilde{\theta}=\tilde{\Theta}_d-\frac{2^{3/2}}{3}\tilde{\eta}^{3/2}$$

The symbols $\tilde{\Theta}_u$ and $\tilde{\Theta}_d$ denote, respectively, the ordinates at which the upgoing and downgoing characteristics through a given point $(\tilde{\eta}, \tilde{\theta})$ intersect the vertical axis. Elimination of $\tilde{\theta}$ between these equations gives

$$\tilde{\eta}=\frac{3^{2/3}}{2^{5/3}}(\tilde{\Theta}_d-\tilde{\Theta}_u)^{2/3} \tag{69}$$

which can be substituted into equation (68) to obtain

$$\frac{dY}{d(x/c)}=\pm\left(\frac{4\tilde{\theta}_w/3}{\tilde{\Theta}_d-\tilde{\Theta}_u}\right)^{1/3} \tag{70}$$

This is the basic relation for the characteristics construction in the physical plane.

The construction of the Mach net itself follows a simple lattice-point procedure (cf. reference 44). By identifying each Mach line with its appropriate value of $\tilde{\Theta}_u$ or $\tilde{\Theta}_d$, the value of $dY/d(x/c)$ at the intersection of any two Mach lines can easily be determined from equation (70) (or its graphical equivalent). The basic construction necessary to locate an unknown point c from the location of two known points a and b is then as indicated in figure 26. The construction

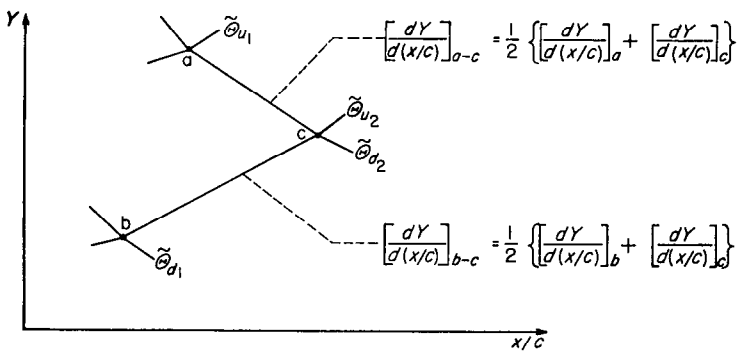

FIGURE 26.—Basic construction for characteristics net.

proceeds rapidly since, as pointed out, variations in the inclination of flow need not be considered in establishing the direction of the Mach lines. Where desired, the value of $\tilde{\theta}$ can be found from the relation

$$\tilde{\theta}=\frac{\tilde{\Theta}_d+\tilde{\Theta}_u}{2} \tag{71}$$

The corresponding value of $\tilde{\eta}$ is given by equation (69).[18]

Figure 27 shows a typical Mach net constructed by stepwise application of the foregoing procedure. This net is for the case of $\tilde{\theta}_w=1.6$ ($\xi_o=0.921$) and corresponds to the flow field shown for the front of the airfoil in figure 3. The construction is begun at the shoulder of the airfoil ($x/c=1/2$, $Y=0$) with the values of $\tilde{\theta}_u$ selected to provide approximately equal spacing between the Mach-lines of the expansion fan. From the shoulder, the construction is carried outward to the sonic line and then inward to the rear surface of the airfoil. The drawing of the Mach-line segments adjoining the sonic line might appear at first to offer some difficulty, since a linear average is obviously unreliable to determine a mean inclination in this vicinity. Actually, no trouble is encountered from this source, since the point at which each Mach line meets the sonic line is already known from the hodograph solution for the subsonic field. The construction of the last segment approaching the sonic line thus reduces to a matter of simply connecting two known points. The slope of the first segment leaving the sonic line is found by either (a) multiplying the slope of the approaching segment by -1, or (b) determining a mean inclination based on the easily demonstrated fact that a Mach line in the vicinity of the sonic line behaves essentially as a semicubical parabola.[19] It is immaterial to the final result which procedure is used. The identity of the Mach lines reflected from the rear surface of the airfoil is determined from equation (71) plus the boundary condition that at this surface $\tilde{\theta}=-\tilde{\theta}_w$. As can be seen by comparing figures 3 and 27, only a relatively small portion of the sonic line need be known to determine conditions on the rear of the airfoil.

REMARKS ON ACCURACY OF SOLUTION

Quantitative statements with regard to the accuracy of the present results are difficult to make. Fortunately, however, a check on the accuracy of the solution is available in the work itself. This check derives from the fact that, in the subsonic portion of the field, the calculated location of a given velocity in the physical plane should, theoretically, be independent of the path of integration which is followed in the hodograph. Thus, for example, the position of the velocity $\tilde{\eta}=0$, $\tilde{\theta}=1$, which defines the point of intersection E of the shock wave and sonic line, should be the same irrespective of whether it is found from equations (62) and (63)

$$\left(\frac{x}{c}\right)_E=\frac{1}{2I_w}\int_{-\infty}^{-1}\tilde{\eta}\psi_{\tilde{\theta}}(\tilde{\eta},0)d\tilde{\eta}+\frac{1}{4I_w}\int_0^{\psi_E}\sqrt{1+\tilde{\eta}}\,d\psi \tag{72}$$

or from equation (64)

$$\left(\frac{x}{c}\right)_E=\frac{1}{2}+\frac{1}{4I_w}\int_{\tilde{\theta}_w}^{1}\psi_{\tilde{\eta}}(0,\tilde{\theta})d\tilde{\theta} \tag{73}$$

[18] In practice, the construction is actually carried out most easily in a plane of $Y/(2\tilde{\theta}_w)^{1/3}$ versus x/c with the slope of the Mach lines given by

$$\frac{d\,[Y/(2\tilde{\theta}_w)^{1/3}]}{d\,(x/c)}=\pm\left(\frac{2/3}{\tilde{\Theta}_d-\tilde{\Theta}_u}\right)^{1/3}$$

This allows a single graph of slope versus $(\tilde{\Theta}_d-\tilde{\Theta}_u)$ to suffice for all values of $\tilde{\theta}_w$. It also provides somewhat more convenient proportions for the construction of the Mach net.

[19] The latter possibility was pointed out to the authors by Gottfried Guderley.

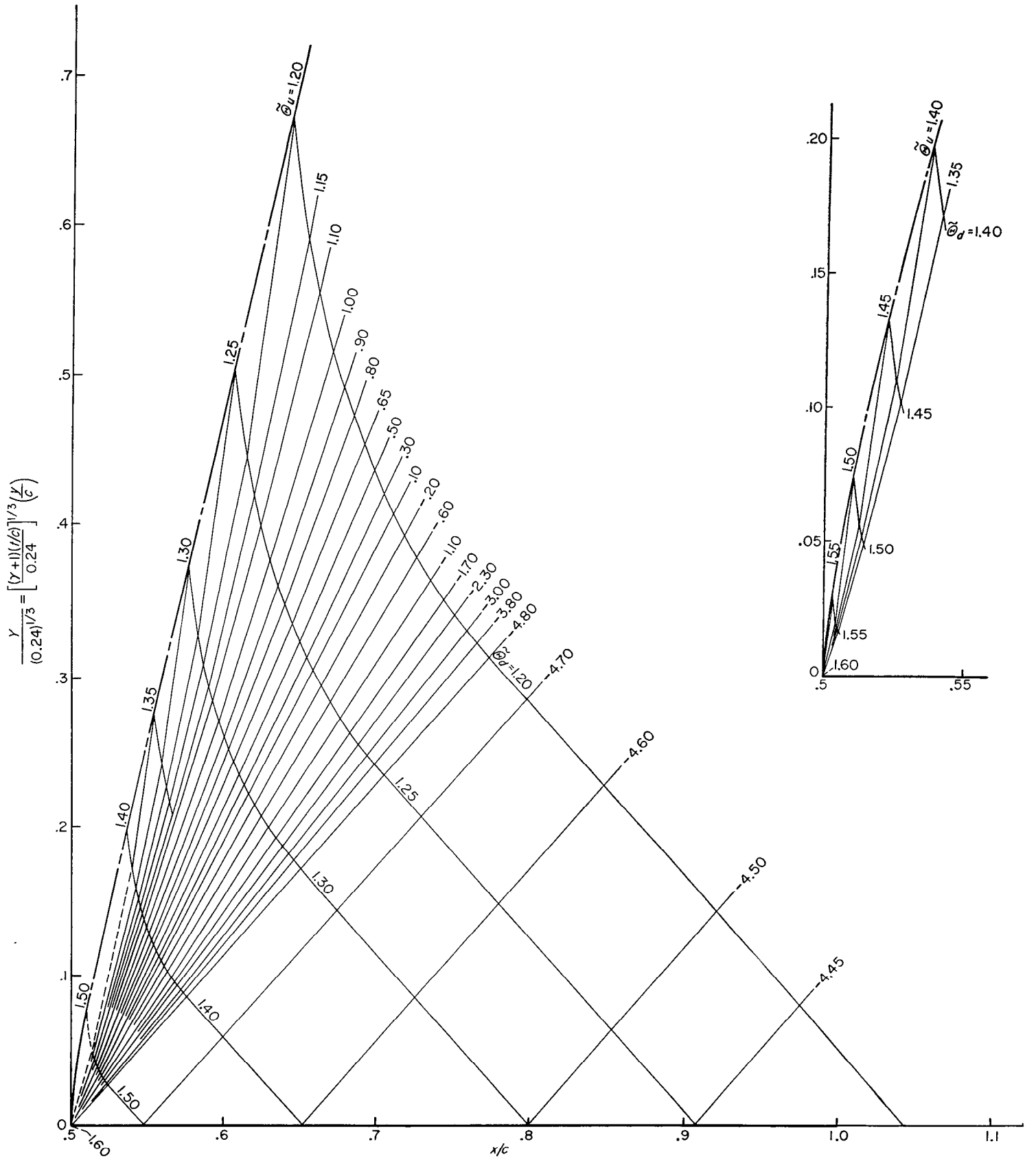

FIGURE 27.—Mach net over rear of airfoil for $\tilde{\theta}_w$=1.6 (ξ_0=0.921).

Actually, as was observed in connection with figure 2, the results of the two determinations show a small discrepancy. Such a result would be expected in any finite-difference solution.

Discrepancies of the type noted can arise from two sources: (1) numerical inaccuracies in the relaxation solution of the finite-difference equations or in the transformation to the physical plane; (2) inaccuracies caused by the fact that the finite-difference equations themselves are not an exact representation of the boundary-value problem for the original partial differential equation. Experience with various refinements in the calculations indicates that the discrepancies here are primarily of the latter origin. Early computations with a coarse lattice and relatively crude finite-difference equations showed a considerable gap between the shock wave and the end of the sonic line. Increasing refinements in the grading of the lattice and in the derivation of certain of the finite-difference equations gave progressive improvement in reducing this gap. This improvement came about primarily as a result of progressive reduction in the value of the integral I_w, the other integrals in equations (72) and (73) being relatively unaffected by the refinements in the calculations. Indications are that, in the results which were taken as final, the values of $|\psi_{\tilde{\sigma}}(\tilde{\eta},\tilde{\theta}_w)|$ and hence of I_w are still somewhat too large. This means (see equation (57b)) that the ordinates of the shock wave and sonic line are probably somewhat smaller than they should be. The same is probably true, in general, of the corresponding values of $|x/c|$. Calculations of the chordwise distribution of $\tilde{\eta}$ on the surface of the airfoil are, however, considerably more precise, since the errors in the two integrals in equation (65) tend to compensate. The refinements in the computations were, in fact, carried to the point where further betterment caused only negligible change in the pressure distribution and over-all drag. Further evidence of the accuracy of the results in this regard is provided by the ease with which the computed values fair into the results of Guderley and Yoshihara at $\xi_o=0$ and into the analytical curves which are available when the bow wave is attached and the flow is completely supersonic (see figs. 5 and 7).

AMES AERONAUTICAL LABORATORY,
NATIONAL ADVISORY COMMITTEE FOR AERONAUTICS,
MOFFETT FIELD, CALIF., *Oct. 8, 1951.*

APPENDIX

EXACT RELATIONS FOR SLOPE OF DRAG CURVE AT A FREE-STREAM MACH NUMBER OF 1

In part I of this report, exact relations are given for the slope of the curve of drag coefficient versus free-stream Mach number at a free-stream Mach number of 1. These relations are based on the fact that at the sonic flight condition the local Mach number M at the surface of an airfoil is stationary with respect to variations in the free-stream Mach number M_o—that is, $(dM/dM_o)_{M_o=1}=0$. The details of the derivation are given in the following paragraphs. The results are not restricted to a double-wedge section but are applicable to the zero-lift drag of a symmetrical profile of any shape.

The general equation for the pressure coefficient, valid for any Mach number and thickness ratio, can be written

$$C_p \equiv \frac{p-p_o}{q_o}=\frac{p-p_o}{q_*}\times\frac{q_*}{q_o}=\frac{2}{\gamma}\left(\frac{p}{p_*}-\frac{p_o}{p_*}\right)\frac{1}{q_o/q_*} \tag{A1}$$

where p is the static pressure at an arbitrary point on the airfoil, p_* and q_* are the static and dynamic pressures at the point on the airfoil at which $M=1$, and p_o and q_o are the static and dynamic pressures in the free stream. When $M_o=1$, conditions in the free stream and at the sonic point are obviously equal ($p_{o_{M_o=1}}=p_{*_{M_o=1}}$, $q_{o_{M_o=1}}=q_{*_{M_o=1}}$) so that

$$C_{p_{M_o=1}}=\frac{2}{\gamma}\left[\left(\frac{p}{p_*}\right)_{M_o=1}-1\right] \tag{A2}$$

Differentiation of equation (A1) with respect to M_o then gives for the rate of change of the pressure coefficient at $M_o=1$

$$\left(\frac{dC_p}{dM_o}\right)_{M_o=1}=\frac{2}{\gamma}\left\{\left[\frac{d(p/p_*)}{dM_o}\right]_{M_o=1}-\left[\frac{d(p_o/p_*)}{dM_o}\right]_{M_o=1}\right\}-C_{p_{M_o=1}}\left[\frac{d(q_o/q_*)}{dM_o}\right]_{M_o=1} \tag{A3}$$

It is now necessary to evaluate the three derivatives on the right-hand side of this equation.

If there are no shock waves present on the surface of the airfoil, the ratio p/p_* can be expressed solely in terms of the local Mach number by an isentropic equation of the form

$$\frac{p}{p_*}=f(M)$$

where the exact nature of the function $f(M)$ is immaterial in the present application. From this equation and from the known fact that $(dM/dM_o)_{M_o=1}=0$, it follows at once that

$$\left[\frac{d(p/p_*)}{dM_o}\right]_{M_o=1}=f'(M)\left(\frac{dM}{dM_o}\right)_{M_o=1}=0 \tag{A4}$$

If there are shock waves present on the airfoil, the argument is slightly more involved, but the same result applies. Equation (A4) states, in effect, that as the free-stream Mach number varies from unity the entire pressure distribution on the surface of the airfoil varies in direct proportion to the pressure at the sonic point.

The derivative $[d(p_o/p_*)/dM_o]_{M_o=1}$, which defines the relative variation between the static pressures in the free stream and at the sonic point, can be found by first expressing the ratio p_o/p_* in terms of the free-stream Mach number M_o. The necessary expression can be obtained either from the

equations for isentropic flow alone ($M_o<1$, no shock wave ahead of the airfoil) or from these equations plus the equations for the normal shock wave ($M_o>1$, detached wave ahead of airfoil). In either case, if the expression is expanded about $M_o=1$ in terms of ascending powers of (M_o^2-1), the result is

$$\frac{p_o}{p_*}=1-\frac{\gamma}{\gamma+1}(M_o^2-1)+0[(M_o^2-1)^2]$$

Differentiation of this equation then gives

$$\left[\frac{d(p_o/p_*)}{dM_o}\right]_{M_o=1}=-\frac{2\gamma}{\gamma+1} \tag{A5}$$

The derivative $[d(q_o/q_*)/dM_o]_{M_o=1}$, which defines the relative variation between the dynamic pressures in the free stream and at the sonic point, can be found by expressing q_o/q_* in terms of known quantities. The necessary relation is given by

$$\frac{q_o}{q_*}=\left(\frac{p_o}{p_*}\right)M_o^2$$

from which it follows that

$$\left[\frac{d(q_o/q_*)}{dM_o}\right]_{M_o=1}=\left[\frac{d(p_o/p_*)}{dM_o}\right]_{M_o=1}+2=-\frac{2}{\gamma+1} \tag{A6}$$

The findings of equations (A4), (A5), and (A6) can now be substituted into the previous equation (A3). The result is the following important relation for the rate of change of the pressure coefficient at the sonic flight speed:

$$\left(\frac{dC_p}{dM_o}\right)_{M_o=1}=\frac{4}{\gamma+1}-\frac{2}{\gamma+1}C_{p_{M_o=1}} \tag{A7}$$

This relation is exact within the limitations of the inviscid theory and is applicable to an airfoil of any shape and thickness ratio.

The drag coefficient of the front portion of any symmetrical airfoil at zero lift can be written

$$c_{d_f}=\int_{-\frac{(t/c)}{2}}^{\frac{(t/c)}{2}}C_p\,d\left(\frac{y}{c}\right)$$

where the integration is carried out over the surface forward of the position of maximum thickness. Differentiation of this equation with respect to M_o and substitution from equation (A7) gives, after integration,

$$\left(\frac{dc_{d_f}}{dM_o}\right)_{M_o=1}=\frac{4}{\gamma+1}\left(\frac{t}{c}\right)-\frac{2}{\gamma+1}(c_{d_f})_{M_o=1} \tag{A8}$$

Similar reasoning gives for the rear portion of the airfoil

$$\left(\frac{dc_{d_r}}{dM_o}\right)_{M_o=1}=-\frac{4}{\gamma+1}\left(\frac{t}{c}\right)-\frac{2}{\gamma+1}(c_{d_r})_{M_o=1} \tag{A9}$$

It follows that for the complete airfoil

$$\left(\frac{dc_d}{dM_o}\right)_{M_o=1}=-\frac{2}{\gamma+1}(c_d)_{M_o=1} \tag{A10}$$

It is apparent from the foregoing derivation that the term proportional to the drag coefficient in each of these equations appears as a consequence of the relative variation between the dynamic pressures in the free stream and at the sonic point. The term proportional to t/c in equations (A8) and (A9) is a result of the relative variation between the corresponding static pressures.

REFERENCES

1. Meyer, Th.: Über zweidimensionale Bewegungsvorgänge in einem Gas, das mit Überschallgeschwindigkeit strömt. Forschungsarbeiten auf dem Gebiete des Ingenieurwesens, VDI, vol. 62, 1908, pp. 31–67.
2. Guderley, K. Gottfried: Considerations of the Structure of Mixed Subsonic-Supersonic Flow Patterns. Tech. Rep. No. F–TR–2168–ND, AAF, Air Matériel Command (Wright Field), Oct. 1947.
3. Maccoll, J. W., and Codd, J.: Theoretical Investigations of the Flow Around Various Bodies in the Sonic Region of Velocities. Theo. Res. Rep. No. 17/45, Armament Res. Dept., British Ministry of Supply, Sept. 1945.
4. Maccoll, J. W.: Investigations of Compressible Flow at Sonic Speeds, Theo. Res. Rep. No. 7/46, Armament Res. Dept., British Ministry of Supply, Sept. 1946.
5. Frankl, F.: On the Problems of Chaplygin for Mixed Sub- and Supersonic Flows. NACA TM 1155, 1947.
6. Busemann, Adolf: A Review of Analytical Methods for the Treatment of Flows With Detached Shocks. NACA TN 1858, 1949.
7. Guderley, G., and Yoshihara, H.: The Flow Over a Wedge Profile at Mach Number 1. Jour. Aero. Sci., vol. 17, no. 11, Nov. 1950, pp. 723–735.
8. Bryson, Arthur Earl, Jr.: An Experimental Investigation of Transsonic Flow Past Two-Dimensional Wedge and Circular-Arc Sections Using a Mach-Zehnder Interferometer. NACA Rep. 1094, 1952. (Formerly NACA TN 2560, 1951.)
9. Griffith, Wayland: Shock-Tube Studies of Transonic Flow Over Wedge Profiles. Jour. Aero. Sci., vol. 19, no. 4, April 1952, pp. 249–257.
10. Liepmann, H. W., and Bryson, A. E., Jr.: Transonic Flow Past Wedge Sections. Jour. Aero. Sci., vol. 17, no. 12, Dec. 1950, pp. 745–755.
11. Busemann, Adolf: Application of Transonic Similarity. NACA TN 2687, 1952.
12. Spreiter, John R.: On the Application of Transonic Similarity Rules. NACA TN 2726, 1952.
13. Tricomi, F.: On Linear Partial Differential Equations of the Second Order of Mixed Type. Trans. A9–T–26, Grad. Div. of Appl. Math., Brown University, 1948.
14. Tsien, Hsue-Shen, and Baron, Judson R.: Airfoils in Slightly Supersonic Flow. Jour. Aero. Sci., vol. 16, no. 1, Jan. 1949, pp. 55–61.
15. von Kármán, Theodore: The Similarity Law of Transonic Flow. Jour. Math. and Phys., vol. XXVI, no. 3, Oct. 1947, pp. 182–190.
16. Kaplan, Carl: On Similarity Rules for Transonic Flows. NACA Rep. 894, 1948. (Formerly NACA TN 1527, 1948.)
17. Liepmann, H. W., Ashkenas, H., and Cole, J. D.: Experiments in Transonic Flow. Tech. Rep. No. 5667, Air Materiel Command, U. S. Air Force, Feb. 1948.
18. Guderley, K. Gottfried: Singularities at the Sonic Velocity. Tech. Rep. F–TR–1171–ND, Air Materiel Command, U. S. Air Force, June 1948.
19. Guderley, Gottfried: Two-Dimensional Flow Patterns With a Free-Stream Mach Number Close to One. AF Tech. Rep. No. 6343, U. S. Air Force, May 1951.
20. Cole, Julian D.: Drag of a Finite Wedge at High Subsonic Speeds. Jour. Math. and Phys., vol. XXX, no. 3, July 1951, pp. 79–93.
21. Trilling, Leon: Transonic Flow Past a Wedge at Zero Angle of Attack. WADC Tech. Rep. No. 52–61, U. S. Air Force, March 1952.
22. Spreiter, John R.: Similarity Laws for Transonic Flows About Wings of Finite Span. NACA TN 2273, 1950.
23. Liepmann, Hans Wolfgang, and Puckett, Allen E.: Introduction to Aerodynamics of a Compressible Fluid. John Wiley and Sons, Inc., 1947.
24. Ivey, H. Reese, Stickle, George W., and Schuettler, Alberta: Charts for Determining the Characteristics of Sharp-Nose Airfoils in Two-Dimensional Flow at Supersonic Speeds. NACA TN 1143, 1947.
25. Green, J. R., and Southwell, R. V.: Relaxation Methods Applied to Engineering Problems. IX—High-Speed Flow of Compressible Fluid Through a Two-Dimensional Nozzle. Phil. Trans. Roy. Soc. London, ser. A, no. 808, vol. 239, April 1944, pp. 367–386.
26. Emmons, Howard W.: The Theoretical Flow of a Frictionless, Adiabatic, Perfect Gas Inside of a Two-Dimensional Hyperbolic Nozzle. NACA TN 1003, 1946.
27. O'Brien, George G., Hyman, Morton A., and Kaplan, Sidney: A Study of the Numerical Solution of Partial Differential Equations. Jour. Math. and Phys., vol. XXIX, no. 4, Jan. 1951, pp. 223–251.
28. Whittaker, E. T., and Watson, G. N.: A Course of Modern Analysis. Cambridge, Eng., The University Press, 1945.
29. Guderley, K. Gottfried: On the Transition from a Transonic Potential Flow to a Flow With Shocks. Tech. Rep. F–TR–2160–ND, AAF, Air Materiel Command (Wright Field), Aug. 1947.
30. Emmons, Howard W.: The Numerical Solution of Partial Differential Equations. Quart. Appl. Math., vol. II, no. 3, Oct. 1944, pp. 173–195.
31. Fox, L.: A Short Account of Relaxation Methods. Quart. Jour. Mech. and Appl. Math., vol. I, pt. 3, Sept. 1948, pp. 253–280.

32. Shaw, F. S.: Numerical Solutions of Boundary Value Problems by Relaxation Methods. Numerical Methods of Analysis in Engineering, L. E. Grinter, ed., MacMillan Co., N. Y., 1949, pp. 49–65.
33. Southwell, R. V.: Relaxation Methods in Theoretical Physics. Oxford, The Clarendon Press, 1946.
34. Bickley, W. G.: Finite Difference Formulae for the Square Lattice. Quart. Jour. Mech. and Appl. Math., vol. I, pt. 1, Mar. 1948, pp. 35–42.
35. Fox, L.: Some Improvements in the Use of Relaxation Methods for the Solution of Ordinary and Partial Differential Equations. Proc., Royal Soc. London, ser. A, vol. 190, no. A 1020, June 17, 1947, pp. 31–59.
36. Woods, L. C.: Improvements to the Accuracy of Arithmetical Solutions to Certain Two-Dimensional Field Problems. Quart. Jour. Mech. and Appl. Math., vol. III, pt. 3, Sept. 1950, pp. 349–363.
37. Watson, G. N.: A Treatise on the Theory of Bessel Functions. 2nd ed., Cambridge, Eng., The University Press, 1948.
38. Wu, Chung-Hua: Formulas and Tables of Coefficients for Numerical Differentiation With Function Values Given at Unequally Spaced Points and Application to Solution of Partial Differential Equations. NACA TN 2214, 1950.
39. Fox, L.: Solution by Relaxation Methods of Plane Potential Problems With Mixed Boundary Conditions. Quart. Appl. Math., vol. II, no. 3, Oct. 1944, pp. 251–257.
40. Fox, L.: The Numerical Solution of Elliptic Differential Equations When the Boundary Conditions Involve a Derivative. Phil. Trans. Roy. Soc. London, ser. A, no. 849, vol. 242, 3 May 1950, pp. 345–378.
41. Jahnke, Eugene, and Emde, Fritz: Tables of Functions With Formulae and Curves. Dover Publications, N. Y., 4th ed., 1945.
42. Tasny-Tschiassny, L.: The Triangulation of a Two Dimensional Continuum for the Purpose of the Approximate Solution of Second-Order Partial Differential Equations. Jour. App. Phys., vol. 20, no. 5, May 1949, pp. 419–424.
43. Magnus, Wilhelm, and Oberhettinger, Fritz: Formulas and Theorems for the Special Functions of Mathematical Physics. Chelsea Publishing Co., N. Y., 1949.
44. Isenberg, J. S.: The Method of Characteristics in Compressible Flow. Part I (Steady Supersonic Flow). Tech. Rep. F–TR–1173–A–ND, Air Materiel Command (Wright Field), Dec. 1947.

TABLE I.—CALCULATED VALUES OF ψ FOR $\tilde{\theta}_w=1.6$ ($\xi_o=0.921$)

$-\tilde{n}$	$\tilde{\theta}$	ψ	$-\tilde{n}$	$\tilde{\theta}$	ψ	$-\tilde{n}$	$\tilde{\theta}$	ψ	$-\tilde{n}$	$\tilde{\theta}$	ψ
0	1.5	198	0.1	1.1	4591	0.45	1.25	1691	1.1	0.3	128
	1.4	527		1.075	5642		1.2	2004		.2	85
	1.3	1013		1.05	7132		1.15	2324		.1	43
	1.25	1359		1.0436	7621		1.1	2621			
	1.2	1822					1.0754	2748	1.2	1.4	98
	1.15	2480	.125	1.125	3971					1.2	176
	1.125	2927		1.1	4763	.5	1.5	394		1.0	219
	1.1	3502		1.075	5822		1.4	811		.8	220
	1.075	4272		1.0523	7130		1.3	1268		.7	207
	1.0625	4773					1.2	1755		.6	187
	1.05	5375	.15	1.25	1928		1.1	2196		.5	161
	1.375	6109		1.2	2559		1.0607	2313		.4	132
	1.025	7040		1.15	3467					.3	101
	1.0125	8267		1.125	4082	.6	1.5	329		.2	68
				1.1	4869		1.4	662		.1	34
.0125	1.0625	5003		1.075	5899		1.3	997			
	1.05	5644		1.0603	6664		1.2	1312	1.3	.6	137
	1.0375	6433					1.1	1552		.5	119
	1.025	7441	.175	1.125	4141		1.0119	1633		.4	99
	1.0125	8782		1.1	4902					.3	76
	1.0062	9656		1.075	5870	.7	1.5	258		.2	52
				1.0673	6223		1.4	511		.1	26
.025	1.125	3168					1.3	750			
	1.1	3805	.2	1.5	389		1.2	957	1.4	1.4	48
	1.075	4666		1.4	875		1.1	1101		1.2	87
	1.0625	5228		1.3	1565		1.0	1149		1.0	110
	1.05	5909		1.25	2042		.9311	1120		.8	114
	1.0375	6751		1.2	2679					.6	101
	1.025	7833		1.15	3567	.8	1.4	377		.4	74
	1.0121	9339		1.125	4148		1.2	689		.2	39
				1.1	4862		1.1	785			
.0375	1.0625	5447		1.0733	5810		1.0	822	1.6	1.4	23
	1.05	6165					.9	798		1.2	42
	1.0375	7057	.225	1.125	4100					1.0	54
	1.025	8205		1.1	4753	.8032	.8	720		.8	57
	1.0179	9025		1.0784	5420					.6	51
						.8581	.7	534		.4	38
.05	1.25	1568	.25	1.25	2092					.2	20
	1.2	2100		1.2	2699	.9	1.0	593			
	1.15	2872		1.15	3504		.9	585	1.8	1.4	10
	1.125	3403		1.125	4005		.8	545		1.2	19
	1.1	4097		1.1	4588		.7	481		1.0	25
	1.075	5041		1.0825	5046					.8	27
	1.0625	5657				.9003	.6	406		.6	24
	1.05	6407	.275	1.125	3868					.4	18
	1.0375	7343		1.1	4379	.9331	.5	307		.2	10
	1.0234	8729		1.0856	4704						
						.9583	.4	228	2.0	1.4	5
.0625	1.0625	5854	.3	1.5	435					1.2	9
	1.05	6630		1.4	948	.9770	.3	162		1.0	11
	1.0375	7691		1.3	1630					.8	12
	1.0288	8440		1.25	2072	.9899	.2	104		.6	12
				1.2	2620					.4	9
.075	1.125	3622		1.15	3301	.9975	.1	52		.2	5
	1.1	4365		1.1	4134						
	1.075	5374		1.0877	4357	1.0	1.4	197			
	1.0625	6034					1.2	352			
	1.05	6830	.35	1.25	1990		1.0	427			
	1.0375	7824		1.2	2460		.9	428			
	1.0339	8158		1.15	3097		.8	407			
				1.1	3618		.7	369			
.0875	1.0625	6194		1.0884	3763		.6	321			
	1.05	6999					.5	267			
	1.0388	7889	.4	1.5	435		.4	211			
				1.4	921						
.1	1.5	395		1.3	1509	1.1	.8	302			
	1.4	720		1.25	1857		.7	279			
	1.3	1337		1.2	2216		.6	247			
	1.25	1764		1.15	2669		.5	210			
	1.2	2356		1.1	3099		.4	170			
	1.15	3220		1.0844	3225						
	1.125	3815									

U. S. GOVERNMENT PRINTING OFFICE: 1953